Spectrochimica Acta Part A: Molecular and Biomolecular Spectroscopy 102 (2013) 99–113

Contents lists available at SciVerse ScienceDirect

Spectrochimica Acta Part A: Molecular and Biomolecular Spectroscopy

journal homepage: www.elsevier.com/locate/saa

Vibrational spectroscopic (FT-IR, FT-Raman, ^{1}H NMR and UV) investigations and computational study of 5-nitro-2-(4-nitrobenzyl) benzoxazole

J.B. Bhagyasree [a], Hema Tresa Varghese [b], C. Yohannan Panicker [c,*], Jadu Samuel [a], Christian Van Alsenoy [d], Kayhan Bolelli [e], Ilkay Yildiz [e], Esin Aki [e]

[a] Department of Chemistry, Mar Ivanios College, Nalanchira, Trivandrum, Kerala, India
[b] Department of Physics, Fatima Mata National College, Kollam, Kerala, India
[c] Department of Physics, TKM College of Arts and Science, Kollam, Kerala, India
[d] Department of Chemistry, University of Antwerp, B2610 Antwerp, Belgium
[e] Faculty of Pharmacy, Department of Pharmaceutical Chemistry, Ankara University, Tandogan 06100, Ankara, Turkey

HIGHLIGHTS

- IR, Raman spectra and NBO analysis were reported.
- The wavenumbers are calculated theoretically using Gaussian09 software.
- The wavenumbers are assigned using PED analysis.
- The geometrical parameters are in agreement with that of similar derivatives.

GRAPHICAL ABSTRACT

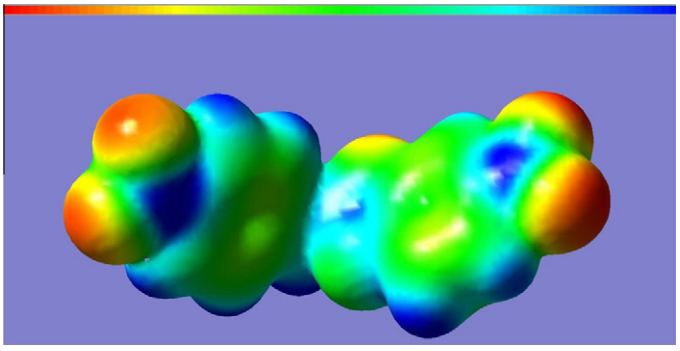

ARTICLE INFO

Article history:
Received 8 June 2012
Received in revised form 30 August 2012
Accepted 9 September 2012
Available online 2 October 2012

Keywords:
FT-IR
FT-Raman
Benzoxazole
Hyperpolarizability
NBO

ABSTRACT

The optimized molecular structure, vibrational frequencies, corresponding vibrational assignments of 5-nitro-2-(4-nitrobenzyl) benzoxazole have been investigated experimentally and theoretically using Gaussian09 software package. Potential energy distribution of the normal modes of vibrations was done using GAR2PED program. The energy and oscillator strength calculated by time dependent density functional theory almost compliments with experimental findings. Gauge-including atomic orbital ^{1}H NMR chemical shifts calculations were carried out by using B3LYP functional with 6-31G* basis set. The HOMO and LUMO analysis is used to determine the charge transfer within the molecule. The stability of the molecule arising from hyper-conjugative interaction and charge delocalization have been analyzed using NBO analysis. MEP was performed by the DFT method and the predicted infrared intensities and Raman activities have also been reported. The calculated geometrical parameters are in agreement with that of similar derivatives.

Introduction

Benzoxazole is a five-membered ring compound containing both nitrogen and oxygen fused to a benzene ring and the recurring structural motifs are found in biologically active compounds [1]. The benzoxazoles have been the aim of many researchers for many years because they constitute an important class of heterocyclic compounds exhibiting substantial chemotherapeutic activities [2,3]. Benzoxazole derivatives exhibit antimicrobial [4–6], antiviral [7,8], multi drug-resistance cancer cell activities [9], with inhibiting activity on eukaryotic topoisomerase II enzyme in cell-

* Corresponding author. Tel.: +91 9895370968.
E-mail address: cyphyp@rediffmail.com (C.Y. Panicker).

1386-1425/$ - see front matter © 2012 Elsevier B.V. All rights reserved.
http://dx.doi.org/10.1016/j.saa.2012.09.032

free system [10–12]. It has been reported that benzoxazole have shown low toxicity in warm-blooded animals [13,14]. Yalcin et al. [15–18] reported the synthesis and microbiological activity of 5-substituted-2-(*p*-substituted phenyl)benzoxazole derivatives. Anto et al. [19] reported the vibrational spectroscopic and *ab initio* calculations of 5-methyl-2-(*p*-fluorophenyl)benzoxazole. Vibrational spectroscopic studies and *ab initio* calculations of 5-methyl-2-(*p*-methylaminophenyl) benzoxazole is reported by Ambujakshan et al. [20]. *Ab initio* quantum mechanical method is at present widely used for simulating IR spectrum. Such simulations are indispensable tools to perform normal coordinate analysis so that modern vibrational spectroscopy is unimaginable without involving them and time-dependent DFT (TD-DFT) calculations have also been used for the analysis of the electronic spectrum and spectroscopic properties. The energies, degrees of hybridization, populations of the lone electron pairs of oxygen, energies of their interaction with the anti-bonding π^* orbitals of the benzene ring and electron density (ED) distributions and $E(2)$ energies have been calculated by NBO analysis using DFT method to give clear evidence of stabilization originating from the hyperconjugation of various intra-molecular interactions. In the previous studies, 5-nitro-2-(4-nitrobenzyl)benzoxazole was synthesized and was tested for various activities. The antihistamine activity of this compound was determined and its percent inhibition against histamine induced contraction was found 11.04 [21]. The antifungal activity against *C. albicans* of the compound was determined and found significantly active (MIC: 6.2 μg/ml) [22]. The reverse transcriptase (RT) inhibitory activity of the title compound was determined and it showed good inhibitory activity as 6×10^4 - μmol/l IC_{50} value [7]. In this work, IR, Raman spectra, ^1H NMR parameters and UV–Vis spectrum of 5-nitro-2-(4-nitrobenzyl) benzoxazole are reported both experimentally and theoretically. The HOMO and LUMO analysis have been used to elucidate information regarding charge transfer within the molecule. There has been growing interest in using organic materials for nonlinear optical (NLO) devices, functioning as second harmonic generators, frequency converters, electro-optical modulators, etc. because of the large second order electric susceptibilities of organic materials. Since the second order electric susceptibility is related to first hyperpolarizability, the search for organic chromophores with large first hyperpolarizability is fully justified. The organic compounds showing high hyperpolarizability are those containing an electron donating group or an electron withdrawing group interacting through a system of conjugated double bonds. In this case, the electron withdrawing group NO_2 is present.

Experimental details

For the synthesis of the benzoxazole derivative, using aqueous mineral acids as the condensation reagent did not provide successful results, because of the oxazole ring which was easily hydrolyzed under these conditions [21]. The title compound 5-nitro-2-(4-nitrobenzyl) benzoxazole were prepared by heating 0.01 mol 2-amino-4-nitrophenol with 0.02 mol *p*-nitrophenylacetic acid in 12 g polyphosphoric acid and stirring for 2.5 h. At the end of the reaction period, the residues were poured into an ice–water mixture and alkalized with 10% NaOH solution extracted with benzene. Then, this solution was dried over anhydrous sodium sulfate and evaporated under diminished pressure. The residue was boiled with 200 mg charcoal in ethanol and filtered. After the evaporation of solvent in vacuum, the crude product was obtained and re-crystallized from methanol [22,23]. The scheme of synthesis is shown below.

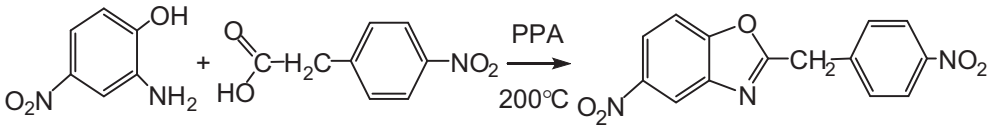

The FT-IR spectrum (Fig. 1) was recorded using KBr pellets on a DR/Jasco FT-IR 6300 spectrometer. The spectral resolution was 2 cm^{-1}. The FT-Raman spectrum (Fig. 2) was obtained on a Bruker RFS 100/s, Germany. For excitation of the spectrum the emission of Nd:YAG laser was used, excitation wavelength 1064 nm, maximal power 150 mW, measurement on solid sample. The spectral resolution after apodization was 2 cm^{-1}.

Chemical formula:$C_{14}H_9N_3O_5$; molecular weight: 299.24; m/z: 299.05 (100.0%), 300.06 (15.4%), 301.06 (2.1%); elemental analysis: calc./found: C 56.19, 56.18; H 3.03, 3.034; N 14.04, 14.05; O 26.73, 26.74. ^1H NMR spectrum was recorded at 400 MHz on a Varian Inova-400 spectrometer and chemical shifts were reported relative to internal TMS. ^1H NMR spectra (Int. TMS, DMSO); δ ppm; 4.650 (s, 2H, —CH_2— protons); 7.711–7.732 (d, 2H, $J_{2',3'}$ *ve* $J_{6',5'}$ = 8.4 Hz 2′,6′ protons); 7.968–7.990 (d, H, $J_{7\text{-}6}$ = 8.8 Hz, 7 proton); 8.244–8.266 (d, 2H, $J_{3',2'}$ *ve* $J_{5',6'}$ = 8.8 Hz, 3′,5′ protons); 8.303–8.331 (dd, H, $J_{6\text{-}7}$ = 8.8 Hz *ve* $J_{6,4}$ = 2.4 Hz, 6 proton); 8.612–8.606 (d, H, $J_{4\text{-}6}$ = 2.4 Hz, 4 proton).

Computational details

Calculations of the title compound are carried out with Gaussian09 program [24] using the HF/6-31G*, B3LYP/6-31G* and SDD basis sets to predict the molecular structure and vibrational wavenumbers. Molecular geometry was fully optimized by Berny's optimization algorithm using redundant internal coordinates. Harmonic vibrational wavenumbers were calculated using the analytic second derivatives to confirm the convergence to minima on the potential surface. The wavenumber values computed at the Hartree–Fock level contain known systematic errors due to the negligence of electron correlation [25]. We therefore, have used the scaling factor value of 0.8929 for HF/6-31G* basis set. The DFT hybrid B3LYP functional and SDD methods tend to overestimate the fundamental modes; therefore scaling factor of 0.9613 has to be used for obtaining a considerably better agreement with experimental data [25]. The Stuttagard/Dresden effective core potential basis set (SDD) [26] was chosen particularly because of

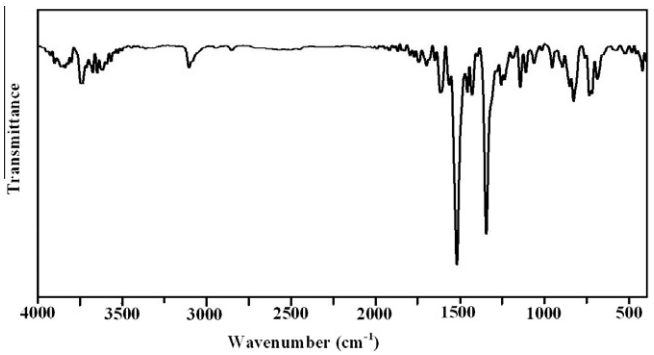

Fig. 1. FT-IR spectrum of 5-nitro-2-(4-nitrobenzyl) benzoxazole.

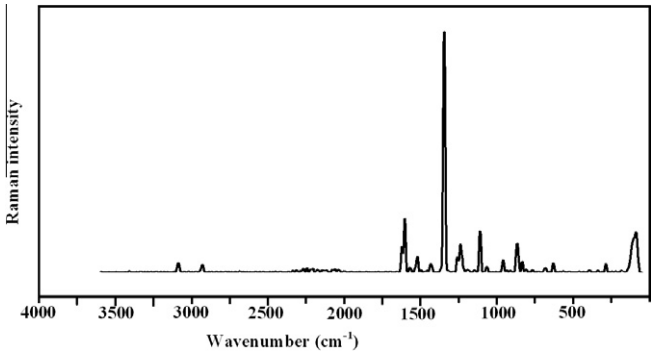

Fig. 2. FT-Raman spectrum of 5-nitro-2-(4-nitrobenzyl) benzoxazole.

its advantage of doing faster calculations with relatively better accuracy and structures [27]. Then frequency calculations were employed to confirm the structure as minimum points in energy. Parameters corresponding to optimized geometry (SDD) of the title compound (Fig. 3) are given in Table 1. The absence of imaginary wavenumbers on the calculated vibrational spectrum confirms that the structure deduced corresponds to minimum energy. In total there are 87 vibrations from (SDD) 3146 to 13 cm^{-1}. The assignments of the calculated wave numbers are aided by the animation option of GAUSSVIEW program, which gives a visual presentation of the vibrational modes [28]. The potential energy distribution (PED) is calculated with the help of GAR2PED software package [29]. The ^{1}H NMR data were obtained from the DFT method using basis set 6-31G*. The characterization of excited states and electronic transitions were performed using the time-dependent DFT method (TD-B3LYP) on their correspondingly optimized ground state geometry. We used the time-dependent density functional theory (TD-DFT), which is found to be an accurate method for evaluating the low-lying excited states of molecules and has been thoroughly applied to solve physical and chemical problems. Vertical excitation energies were computed for the first 30 singlet excited states, in order to reproduce the experimental electronic spectra. Potential energy surface scan studies have been carried out to understand the stability of planar and non-planar structures of the molecule. The HOMO and LUMO are calculated by B3LYP/SDD method.

Results and discussion

IR and Raman spectra

The observed IR, Raman bands and calculated wavenumbers (scaled) and assignments are given in Table 2. The most character-

Table 1
Optimized geometrical parameters (SDD) of 5-nitro-2-(4-nitrobenzyl) benzoxazole, atom labeling according to Fig. 3.

Bond angles (Å)		Bond lengths (°)		Dihedral angles (°)	
C_1—C_2	1.4058	A(2,1,6)	123.7	D(6,1,2,7)	−180.0
C_1—C_6	1.4171	A(2,1,29)	118.2	D(29,1,2,3)	180.0
C_1—N_{29}	1.4789	A(6,1,29)	118.1	D(2,1,6,9)	−179.9
C_2—C_3	1.3981	A(1,2,3)	115.8	D(29,1,6,5)	−179.9
C_2—H_7	1.0829	A(1,2,7)	121.3	D(2,1,29,31)	−179.8
C_3—C_4	1.4183	A(3,2,7)	122.9	D(6,1,29,30)	−179.8
C_3—N_{11}	1.4200	A(2,3,4)	120.5	D(1,2,3,11)	−180.0
C_4—C_5	1.3954	A(2,3,11)	130.8	D(7,2,3,4)	180.0
C_4—O_{10}	1.3980	A(4,3,11)	108.7	D(2,3,4,10)	−179.9
C_5—C_6	1.4037	A(3,4,5)	123.7	D(11,3,4,5)	179.9
C_5—H_8	1.0838	A(3,4,10)	107.5	D(2,3,11,12)	179.9
C_6—H_9	1.0836	A(5,4,10)	128.8	D(3,4,5,8)	180.0
O_{10}—C_{12}	1.4297	A(4,5,6)	116.1	D(10,4,5,6)	179.9
N_{11}—C_{12}	1.3097	A(4,5,8)	122.1	D(5,4,10,12)	−179.9
C_{12}—C_{13}	1.4945	A(6,5,8)	121.8	D(4,5,6,9)	179.9
C_{13}—H_{14}	1.0960	A(1,6,5)	120.1	D(8,5,6,1)	−180.0
C_{13}—H_{15}	1.0954	A(1,6,9)	118.8	D(4,10,12,13)	−178.5
C_{13}—C_{16}	1.5302	A(5,6,9)	121.1	D(3,11,12,13)	178.3
C_{16}—C_{17}	1.4137	A(4,10,12)	104.3	D(10,12,13,14)	−161.0
C_{16}—C_{18}	1.4105	A(3,11,12)	105.8	D(10,12,13,15)	−44.5
C_{17}—C_{19}	1.4016	A(10,12,11)	113.7	D(10,12,13,16)	78.0
C_{17}—H_{20}	1.0872	A(10,12,13)	116.9	D(11,12,13,14)	20.8
C_{18}—C_{21}	1.4039	A(11,12,13)	129.4	D(11,12,13,15)	137.2
C_{18}—H_{22}	1.0869	A(12,13,14)	106.9	D(11,12,13,16)	−100.3
C_{19}—C_{23}	1.4064	A(12,13,15)	109.1	D(12,13,16,17)	58.2
C_{19}—H_{24}	1.0842	A(12,13,16)	112.8	D(12,13,16,18)	−122.8
C_{21}—C_{23}	1.4045	A(14,13,15)	108.0	D(14,13,16,17)	−61.1
C_{21}—H_{25}	1.0842	A(14,13,16)	110.0	D(14,13,16,18)	117.9
C_{23}—N_{26}	1.4775	A(15,13,16)	110.0	D(15,13,16,17)	180.1
N_{26}—O_{27}	1.2791	A(13,16,17)	120.1	D(13,16,17,19)	179.0
N_{26}—O_{28}	1.2794	A(13,16,18)	120.5	D(18,16,17,20)	−180.0
N_{29}—O_{30}	1.2786	A(17,16,18)	119.4	D(13,16,18,21)	−179.0
N_{29}—O_{31}	1.2791	A(16,17,19)	120.7	D(13,16,18,22)	1.2
		A(16,17,20)	119.7	D(17,16,18,22)	−179.7
		A(19,17,20)	119.6	D(16,17,19,24)	−179.9
		A(16,18,21)	120.8	D(20,17,19,23)	180.0
		A(16,18,22)	119.8	D(16,18,21,25)	−180.0
		A(21,18,22)	119.4	D(22,18,21,23)	179.8
		A(17,19,23)	118.6		
		A(17,19,24)	121.7		
		A(23,19,24)	119.7		
		A(18,21,23)	118.5		
		A(18,21,25)	121.8		
		A(23,21,25)	119.7		
		A(19,23,21)	122.0		
		A(19,23,26)	119.0		
		A(21,23,26)	119.0		
		A(23,26,27)	118.1		
		A(23,26,28)	118.1		
		A(27,26,28)	123.8		
		A(1,29,30)	118.1		
		A(1,29,31)	118.1		
		A(30,29,31)	123.8		

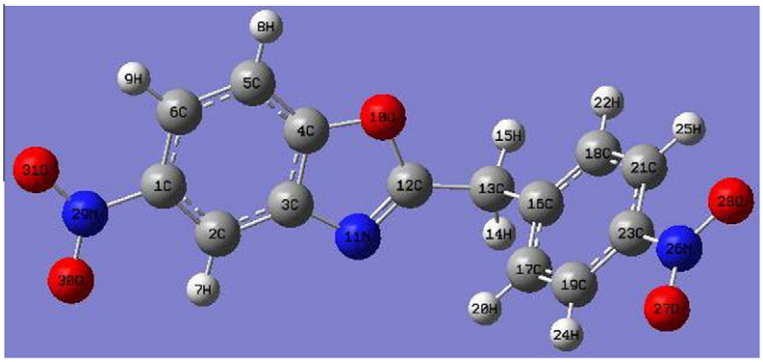

Fig. 3. Optimized geometry (B3LYP/SDD) of 5-nitro-2-(4-nitrobenzyl) benzoxazole.

istic bands in the spectra of nitro compounds are due to the NO_2 stretching vibrations. In nitro compounds NO_2 stretching vibrations are located in the regions 1550–1300 cm^{-1} [30,31]. Nitrobenzene derivatives display $\upsilon_{as}NO_2$ in the region 1535 ± 30 cm^{-1} and 3-nitropyridines at 1530 ± 10 cm^{-1} [30,32] and in substituted nitro benzenes [30,31] υ_sNO_2 appears strongly at 1345 ± 30 cm^{-1}, in 3-nitropyridine at 1350 ± 20 cm^{-1} and in conjugated nitroalkenes [33] at 1345 ± 15 cm^{-1}. For the title compound, SDD calculations give NO_2 stretching vibrations at 1415, 1391, 1374 and 1352 cm^{-1}. The bands observed at 1398, 1347 cm^{-1} in the IR spectrum and at 1387 cm^{-1} in Raman spectrum was assigned as NO_2 stretching modes. The NO_2 scissors [30] occur at higher wavenumbers (850 ± 60 cm^{-1}) when conjugated to C—C or aromatic molecules and according to some investigators [34,35] with a contribution of υCN which is expected near 1120 cm^{-1}. For nitrobenzene, δNO_2 is reported [30] at 852 cm^{-1}, for H_2CCHNO_2 at 890 cm^{-1} and 1,3-dinitrobenzene at 904 and 834 cm^{-1}. For the title compound, the band observed at 767 cm^{-1} in the Raman spectrum, 761 cm^{-1} in the IR spectrum and at 772, 759 cm^{-1} (SDD) are assigned as δNO_2 modes. In aromatic compounds, the wagging mode ωNO_2 is expected in the region 740 ± 50 cm^{-1} with a moderate to strong intensity, a region in which γCH is also active [30]. ωNO_2 is reported at 701 and 728 cm^{-1} for 1,2-dinitrobenzene and at 710 and 772 cm^{-1} for 1,4-dinitrobenzene [30]. For the title compound, the band at 688 cm^{-1} in the IR spectrum and 683 cm^{-1} in the Raman spectrum is assigned as ωNO_2 mode. The SDD calculation gives 699 and 663 cm^{-1} as ωNO_2 modes. The rocking mode ρNO_2 is active in the region 540 ± 70 cm^{-1} in aromatic nitro compounds [30]. Varsanyi et al. [36] and Suryanarayana et al. [37] reported the ranges 70 ± 20 and 65 ± 10 cm^{-1} respectively, as the torsion mode of NO_2 for aromatic compounds. In the present case, the deformation modes of NO_2 are assigned at 522, 441 cm^{-1} (SDD) and at 524, 458 cm^{-1} in IR spectrum.

The C=N stretching skeletal bands are expected in the range 1672–1566 cm^{-1} [19,38–40]. Saxena et al. [38] reported a value 1608 cm^{-1} for poly benzodithiazole and Klots and Collier [41] reported a value 1517 cm^{-1} for benzoxazole as C=N stretching mode. The bands observed at 1520 cm^{-1} in both spectra and 1536 cm^{-1} given by calculation is assigned as υC=N for the title compound. The C—N stretching vibrations are observed in the region 1330–1260 cm^{-1} due to stretching of the phenyl carbon—nitrogen bond [42]. For 2-mercapto benzoxazole this mode [43] reported at 1340 cm^{-1} (Raman) and 1325 cm^{-1} (*ab initio* calculations). Sandhyarani et al. [44] reported υCN at 1318 cm^{-1} for 2-mercaptobenzothiazole. In the present case, the SDD calculations give 1228, 1219 and 1195 cm^{-1} as C—N stretching modes with a band at 1192 cm^{-1} in the Raman spectrum.

The vibrations of the CH_2 group, the asymmetric stretch $\upsilon_{as}CH_2$, symmetric stretch υ_sCH_2, scissoring vibration δCH_2 and wagging vibration ωCH_2 appear in the regions 3000 ± 50, 2965 ± 30, 1455 ± 55 and 1350 ± 85 cm^{-1}, respectively [30,42]. The SDD calculations give $\upsilon_{as}CH_2$ at 3022 cm^{-1} and υ_sCH_2 at 2966 cm^{-1}. The bands at 2949 in IR spectrum and 2973 cm^{-1} in Raman spectrum are assigned as CH_2 symmetric stretching modes for the title compound. For the title compound, the scissoring mode of the CH_2 group is assigned at 1438 (SDD), 1428 (IR) and at 1433 cm^{-1} (Raman). The CH_2 wagging mode is observed at 1282 cm^{-1} in the IR spectrum and at 1288 cm^{-1} theoretically. The band at 1233 cm^{-1} in the IR spectrum, 1237 cm^{-1} in the Raman spectrum and at 1239 cm^{-1} (SDD) is assigned as the twisting mode τCH_2. The rocking mode [30] ρCH_2 is expected in the range 895 ± 85 cm^{-1}. The band at 951 cm^{-1} in the IR spectrum, at 960 cm^{-1} in the Raman spectrum and at 947 cm^{-1} (SDD) is assigned as ρCH_2 mode for the title compound.

As expected the asymmetric C—O—C vibration is assigned at 1144 cm^{-1} in IR spectrum and at 1146 cm^{-1} in the Raman spectrum with SDD value at 1153 cm^{-1}. The symmetric C—O—C stretching vibration is assigned at 1079 cm^{-1} theoretically and observed at 1063 in the IR spectrum and at 1066 cm^{-1} in the Raman spectrum of the title compound. The C—O—C stretching is reported at 1250 and 1073 cm^{-1} for 2-mercaptobenzoxazole [39,43].

The existence of one or more aromatic rings in the structure is normally readily determined from the C—H and C=C—C ring related vibrations. The C—H stretching mode occur above 3000 cm^{-1} and is typically exhibited as a multiplicity of weak to moderate bands, compared with the aliphatic C—H stretch [45]. Klot and Collier [41] reported the bands at 3085, 3074, 3065 and 3045 cm^{-1} as υCH modes for benzoxazole. The bands observed at 3105, 3086 cm^{-1} in the IR spectrum and at 3124, 3106, 3086 cm^{-1} in the Raman spectrum are assigned as the C—H stretching modes of the phenyl rings. The SDD calculations give these modes in the range 3087–3146 cm^{-1}. The benzene ring possesses six ring stretching vibrations, of which the four with the highest wave numbers (occurring near 1600, 1580, 1490 and 1440 cm^{-1}) are good group vibrations. In the absence of ring conjugation, the band near 1580 cm^{-1} is usually weaker than that at 1600 cm^{-1}. The fifth ring stretching vibration which is active near 1335 ± 35 cm^{-1} a region which overlaps strongly with that of the CH in-plane deformation and the intensity is in general, low or medium high [30]. The sixth ring stretching vibration or ring breathing mode appears as a weak band near 1000 cm^{-1} in mono, 1,3-di and 1,3,5-trisubstituted benzenes. In the other wise substituted benzene, however, this vibration is substituent sensitive and is difficult to distinguish from the ring in-plane deformation.

Since the identification of all the normal modes of vibrations of large molecules is not trivial, we tried to simplify the problem by considering each molecule as substituted benzene. Such an idea has already been successfully utilized by several workers for the vibrational assignments of molecules containing multiple homo- and hetero-aromatic rings [46,47–50]. In the following discussion, the phenyl rings attached with 1,2,4-tri heavy substitution and para substitution are assigned as PhI and PhII, respectively and the benzoxazole ring as RingIII. The modes in the two phenyl rings will differ in wave number and the magnitude of splitting will depend on the strength of interactions between different parts (internal coordinates) of the two rings. For some modes, this splitting is so small that they may be considered as quasi-degenerate and for the other modes a significant amount of splitting is observed. Such observations have already been reported [46–48,51].

For the title compound, the bands observed at 1612, 1432, 1398 cm^{-1} in the IR spectrum, 1602, 1387 cm^{-1} in the Raman spectrum and at 1602, 1590, 1439, 1391, 1308 cm^{-1} (SDD) are assigned as υPhI modes. In asymmetric tri-substituted benzene, when all the three substituents are light, the ring breathing mode falls in the range 500–600 cm^{-1}; when all the three substituents are heavy, it appears in the range 1050–1100 cm^{-1} and in the case of mixed substituents, it falls in the range 600–750 cm^{-1} [52]. Madhavan et al. [53] reported the ring breathing mode for a compound having two tri-substituted benzene rings at 1110 cm^{-1} and 1083 cm^{-1}. For the title compound, PED analysis gives the ring breathing mode at 1040 cm^{-1} [54]. For the phenyl ring PhI, the bands observed at 1254, 1144, 1112 cm^{-1} in the IR spectrum and at 1256, 1146, 1112 cm^{-1} in the Raman spectrum are assigned as in-plane CH deformation modes. SDD calculations give these modes at 1247, 1153, 1112 cm^{-1} which are in agreement with the literature [30] and for tri-substituted benzenes δCH modes are expected in the range 1050–1280 cm^{-1} [30].

For para substitued benzenes, the δCH modes are expected in the range 995–1315 cm^{-1} [30]. Bands observed at 1187, 1014 cm^{-1} in the IR spectrum are assigned as δCH modes for the ring PhII. The corresponding theoretical values (SDD) are 1308, 1181, 1099 and 1002 cm^{-1}. For the para-substituted phenyl ring,

Table 2
IR, Raman bands and calculated (scaled) wavenumbers of 5-nitro-2-(4-nitrobenzyl) benzoxazole and assignments.

HF/6-31G*			B3LYP/6-31G*			B3LYP/SDD			IR	Raman	Assignments[a]
$\upsilon(cm^{-1})$	IR_I	R_A	$\upsilon(cm^{-1})$	IR_I	R_A	$\upsilon(cm^{-1})$	IR_I	R_A	$\upsilon(cm^{-1})$	$\upsilon(cm^{-1})$	
3079	12.53	51.81	3152	8.34	54.04	3146	9.26	67.56	–	–	υCH I(99)
3073	5.53	85.43	3144	4.15	97.48	3141	2.92	79.65	–	–	υCH I(99)
3066	3.37	107.63	3137	2.82	118.33	3132	3.69	123.05	–	–	υCH II(96)
3065	2.64	24.48	3136	1.05	27.11	3130	0.38	16.92	–	–	υCH II(97)
3056	1.69	49.47	3127	1.69	59.23	3124	1.82	41.71	–	3124	υCH I(99)
3022	6.21	65.12	3091	3.38	69.90	3090	5.67	59.95	3105	3106	υCH II(97)
3016	4.16	46.11	3090	7.76	52.53	3087	6.19	41.83	3086	3086	υCH II(97)
2941	1.39	60.83	3007	2.38	72.20	3022	3.10	60.10	–	–	$\upsilon_{as}CH_2$(100)
2889	6.29	116.14	2958	4.90	156.58	2966	7.36	180.19	2949	2973	$\upsilon_{s}CH_2$(100)
1638	97.94	111.77	1611	36.57	109.39	1602	36.99	92.12	1612	1602	υPhI(69), υCN(10)
1623	18.38	93.26	1601	4.97	184.79	1590	10.59	264.36	–	–	υPhI(67)
1616	62.26	121.52	1594	54.48	154.66	1585	62.31	145.82	–	–	υPhII(68), υPhI(17)
1607	25.40	1.70	1588	3.59	2.09	1578	3.73	1.88	1561	1571	υPhII(78)
1594	60.58	26.08	1546	58.55	103.36	1536	67.09	112.94	1520	1520	υC=N(60), υPhI(16)
1506	10.86	13.09	1491	9.53	8.05	1468	7.54	14.35	1456	1459	δCHII(18), υPhII(78)
1474	113.13	16.72	1458	40.03	16.83	1439	24.06	20.61	1432	–	υPhI(72), δCHI(17)
1461	16.69	27.35	1454	17.47	32.19	1438	32.19	38.95	1428	1433	δCH_2(91)
1455	140.60	3.12	1436	96.82	4.53	1415	78.76	23.99	–	–	$\upsilon_{as}NO_2$(58), υPhII(17)
1449	260.96	0.18	1432	69.65	22.39	1413	79.09	13.41	–	–	υPhII(70), $\upsilon_{as}NO_2$(16)
1400	127.81	8.49	1406	36.76	17.23	1391	45.93	13.11	1398	1387	$\upsilon_{as}NO_2$(52), υPhI(47)
1397	155.29	0.74	1397	48.87	3.93	1374	54.92	6.78	–	–	$\upsilon_{s}NO_2$(55), δCHII(17),
1340	5.53	5.05	1366	25.50	19.45	1352	49.77	18.84	1347	–	υPhI(16), $\upsilon_{s}NO_2$(55)
1327	53.70	73.09	1343	9.59	7.97	1342	18.62	5.83	1345	1345	δCH_2(14), υPhII(60)
1324	169.26	277.47	1324	5.36	1.35	1308	8.73	2.98	–	–	δCHII(49), υPhI(44)
1322	403.97	161.40	1301	3.18	6.17	1288	1.24	3.57	1282	–	δCH_2(62), υPhII(12)
1299	28.27	16.36	1259	0.12	10.90	1247	3.63	18.25	1254	1256	δCHI(58), υC—O(12)
1270	52.70	13.28	1251	74.70	52.99	1239	71.76	65.19	1233	1237	δCH_2(67), δCHI(13)
1258	3.22	8.71	1241	216.92	492.24	1228	215.79	565.21	–	–	υCN(65), υNO_2 (17)
1230	83.73	9.59	1233	417.50	296.87	1219	406.26	386.74	–	–	υNO_2 (43) υCN(48)
1214	63.22	119.99	1203	23.00	159.96	1195	17.06	122.93	–	1192	υC—N(77), υPhI(19)
1193	10.83	7.61	1188	31.45	25.16	1181	11.88	18.38	1187	–	δCHII(72), υC—C(14)
1184	12.10	2.25	1182	7.82	8.73	1172	29.88	24.75	–	–	υCC(32), δCH II(22), υPhII(25)
1172	15.57	4.42	1167	1.35	5.87	1153	3.38	4.39	1144	1146	δCHI(55), υC—O(42)
1135	18.60	8.03	1127	33.26	3.85	1112	42.76	3.11	1112	1112	δCHI(65), υPhI(17)
1114	32.69	10.91	1112	4.04	2.76	1099	3.04	3.26	–	–	δCHII(59), υPhII(28)
1108	7.27	33.74	1097	32.90	30.38	1084	46.15	24.18	–	–	υCN(28) δCHII(22), υPhII(21)
1106	3.29	6.31	1090	44.75	29.76	1079	25.68	38.45	1063	1066	υCC(11) υC—O(51)
1062	18.74	8.35	1048	29.01	7.37	1040	32.85	11.74	–	–	δCHI(22) υCN(19) υPhI(51)
1053	0.86	2.97	1014	9.73	2.97	1002	0.04	0.47	1014	–	δCHII(56), υPhII(32)
1048	0.94	1.47	994	0.66	3.15	996	8.66	5.46	–	–	γCHII(74), τPhII(17)
1037	0.14	0.14	983	0.77	0.42	992	1.99	0.13	–	–	γCHII(83)
1017	7.29	1.85	976	0.87	0.48	984	0.42	0.36	–	–	γCHI(86)
991	29.63	0.36	953	11.76	9.10	947	13.65	6.16	951	960	δCH_2(79), δPhI(14)
961	13.90	9.45	930	23.72	0.90	941	29.11	0.29	930	935	γCHI(79), τPhI(10)
916	5.31	3.32	909	1.21	2.45	896	1.66	3.71	892	900	γRingIII(35), δCH_2(24), δPhI(21)
912	18.47	3.77	867	15.63	5.19	868	20.62	6.17	852	867	γCHII(65)
889	25.41	12.24	847	0.41	3.71	854	0.46	0.84	–	–	γCHII(97)
884	0.21	1.98	842	10.04	38.00	841	38.85	0.16	–	–	υO—C(40),δRingIII(25)
876	49.13	1.52	835	31.62	2.76	830	17.22	39.36	828	833	γCHI(81) τPhI(11)
833	9.95	36.43	823	7.36	33.82	812	46.20	20.42	–	–	δPhII(34),υCC(21), υC—O(13)
831	84.92	3.20	814	95.17	16.53	805	54.85	46.33	–	808	υO—C(37), δPhII(5)
806	19.97	13.71	781	19.42	4.36	772	11.79	4.77	–	767	δNO_2 (41), τPhII(24),δPhII(15)
803	58.93	7.62	778	50.00	5.92	759	49.05	5.31	761	–	δNO_2 (46),δRingIII(21) δPhI(19)
768	0.97	0.70	750	7.27	5.34	756	1.98	0.85	–	–	τPhII(41), δNO_2 (22)
763	15.22	4.97	736	0.78	0.74	738	13.23	6.06	735	–	υPhII(60), γRingIII(26)
728	41.31	7.23	703	20.61	6.87	708	26.19	6.07	–	–	τPhII(36), δCN(10), γRingIII(18) γCN(10)
718	39.90	2.99	693	26.48	3.66	699	33.78	3.74	688	683	γNO_2 (41), γCN(17), τPhII(12)
690	19.66	3.35	675	22.10	2.04	663	15.51	4.22	–	–	δRingIII(42) γNO_2 (51)
686	33.62	1.73	670	1.66	6.97	661	12.92	3.22	–	–	δPhII(22) δPhI(21), δRingIII(21), γRingIII(20)

(*continued on next page*)

Table 2 (*continued*)

HF/6-31G*			B3LYP/6-31G*			B3LYP/SDD			IR	Raman	Assignments[a]
υ(cm^{-1})	IR_I	R_A	υ(cm^{-1})	IR_I	R_A	υ(cm^{-1})	IR_I	R_A	υ(cm^{-1})	υ(cm^{-1})	
675	12.08	6.90	664	14.49	2.58	657	16.28	5.91	650	–	γCN(34) τPhII(33) γRingIII(17)
640	1.09	6.70	637	0.53	8.05	622	0.70	9.43	618	630	δPhII(79)
619	4.77	1.88	610	2.50	3.55	599	3.65	4.15	594	–	γRingIII(30) δPhI(23), δNO_2 (19), τPhII(15)
580	1.67	0.93	569	0.74	1.71	563	1.04	1.44	575	–	τPhI(45) γCN(17), γRingIII(18)
560	4.25	4.90	555	2.17	6.07	548	3.32	7.57	–	–	δPhI(28), γRingII(21), τPhI(22)
535	9.87	0.38	532	4.90	1.19	522	4.48	1.15	524	–	τNO_2 (40), δCN(17),δPhI(18)
515	4.37	1.16	511	1.28	3.06	500	1.25	3.86	–	–	δCN(79)
492	6.51	0.66	480	3.47	0.61	475	6.04	0.79	483	–	τPhII(39), δCN(20) γCC(18)
453	2.33	0.22	445	1.29	1.06	441	2.44	0.55	458	–	δCC(14), τNO_2 (43) τPhII(21)
441	3.40	0.97	432	1.70	0.88	429	2.25	1.89	420	–	τPhI(53) τRingIII(20)
421	0.04	0.04	415	0.16	0.07	408	0.09	0.04	–	–	τPhII(83)
401	9.30	1.25	399	5.38	1.89	393	5.62	2.04	–	–	τPhI(29), τPhII(30),δPhII(28)
355	5.25	1.75	352	2.77	1.34	345	2.78	1.55	–	–	δCC(20), δPhI(29),δPhII(28)
340	2.42	2.19	330	1.20	1.11	327	1.56	1.46	–	–	δCC(18) γRingIII(26), γCN(13)
335	3.43	3.61	323	2.16	4.19	318	2.45	3.79	–	–	δCC(13), δPhI(11),γCN(17),γRingIII(27)
285	0.81	0.90	279	0.95	1.14	277	0.69	0.98	–	285	τPhI(51) γRingIII(13), γCN(10)
280	2.96	3.30	277	2.87	2.22	273	2.64	2.43	–	–	δCN(26), δCC(13),τPhI(16)
260	1.73	2.75	256	1.39	2.76	251	1.51	2.34	–	–	δCC(33), δCN(41)
215	4.81	1.22	209	2.23	1.07	204	2.25	1.05	–	–	δCN(44) δCN(16),δCC(10)
176	7.20	1.37	173	4.49	1.62	171	4.42	1.60	–	–	τPhI(17) γRingIII(22), γCN(15),τRingIII(16)
140	2.97	0.95	143	2.36	0.55	140	2.31	0.58	–	–	δCN(40), δCC(37)
111	2.78	0.30	106	1.59	0.62	105	1.50	0.57	–	–	τPhII(17) δCH_2(13),τPhI(18),γCN(17)
80	0.74	0.37	81	0.48	0.18	80	0.50	0.09	–	88	τPhII(29), τCN(24),τRingIII(24)
54	0.03	67		0.32	65		0.01	0.12	–		τCN(88)
50	0.42	0.39	59	0.32	0.30	56	0.37	0.31	–	–	τCN(76) τPhI(16)
24	0.97	9.06	25	0.29	13.10	23	0.28	10.63	–	–	τCH_2(37), γCC(16), τPhII(17), τRingIII(15)
17	2.39	4.32	19	0.84	8.84	19	0.77	7.21	–	–	τCH_2(47), γCC(23)
13	0.57	11.16	16	2.00	5.62	13	2.27	6.57	–	–	τCH_2(66), γCC(20)

[a] abbreviations: υ-stretching; δ-in-plane deformation; γ-out-of-plane deformation; τ-twisting; as-asymmetric; s-symmetric; PhI-1,2,4-tri substituted benzene ring; PhII-para substituted benzene ring; RingIII-benzoxazole ring;% of PED is given in the brackets; IR_I-IR intensity; R_A-Raman activity.

the ring stretching modes are expected in the range 1280–1620 cm^{-1} [30]. In this case υPhII modes are assigned at 1585, 1578, 1468, 1413, 1342 cm^{-1} theoretically (SDD) and observed at 1561, 1456, 1345 cm^{-1} in the IR spectrum and at 1571, 1459, 1345 cm^{-1} in the Raman spectrum. The ring breathing mode for the para-substituted benzenes with entirely different substituents [52] have been reported to be strongly IR active with typical bands in the interval 740–840 cm^{-1}. For the title compound, this is confirmed by the strong band in the infrared spectrum at 735 cm^{-1} which finds support from the computational value 738 cm^{-1}. Ambujakshan et al. [20] reported a value 792 cm^{-1} (IR) and 782 cm^{-1} (HF) as ring breathing mode of para substituted benzene derivative.

The C—H out-of-plane deformations γCH are observed between 1000 and 700 cm^{-1} [30]. γCH vibrations are mainly determined by the number of adjacent hydrogen atoms on the ring. Although strongly electron attracting substituent groups, such as nitro-, can result in an increase (about 30 cm^{-1}) in the frequency of the vibration, these vibrations are not very much affected by the nature of the substituents. 1,2,4-Tri-substituted benzenes show a medium absorption in the range 940–840 cm^{-1} and a strong band in the region 780–760 cm^{-1}. In Raman spectra, the out of plane bands are usually weak [55]. Generally the C—H out-of-plane deformations with the highest wave numbers have a weaker intensity than those absorbing at lower wave numbers. The out-of-plane γCH modes are observed at 930, 828 cm^{-1} in the IR spectrum 935, 833 cm^{-1} in the Raman spectrum for PhI and at 852 cm^{-1} in the IR spectrum, 867 cm^{-1} in Raman spectrum for PhII. The corresponding SDD values are 984, 941, 830 cm^{-1} for PhI and 996, 992, 868, 854 cm^{-1} for PhII. A very strong CH out-of plane deformation band, occurring at 840 ± 50 cm^{-1} is typical for 1,4-disubstituted benzenes [30]. For the title compound, a very strong γCH is observed at 852 cm^{-1} in IR spectrum. Again according to the literature [30,42] a lower γCH absorbs in the neighborhood 820 ± 45 cm^{-1}, but is much weaker or infrared inactive and the corresponding theoretical mode is 854 cm^{-1} .

The benzoxazole ring stretching vibrations exist in the range 1504–1309 cm^{-1} in both spectra [38,56]. Klots and Collier [41] reported the bands at 1615, 1604, 1475 and 1451 cm^{-1} as fundamental ring vibrations of the benzoxazole ring. For benzoxazole, Klots and Collier [41] reported the bands at 932, 847 and 746 cm^{-1} as out-of-plane deformations for the benzene ring. According to Collier and Klots [57] the non-planar vibrations are observed at 970, 932, 864, 847, 764, 620, 574, 417, 254, 218 cm^{-1} for benzoxazole and at 973, 939, 856, 757, 729, 584, 489, 419, 207, 192 cm^{-1} for benzothiazole. The planar modes below 1000 cm^{-1} for benzoxazole are reported to be at 920, 870, 778, 622, 538, 413 cm^{-1} and for benzothiazole at 873, 801, 712, 666, 531, 504, 530 cm^{-1} [57]. We have also observed the planar and non-planar modes for the title compound in this region.

Optimized geometry

The optimized molecular structure of 5-nitro-(2-*p*-nitrobenzyl) benzoxazole was determined by using Gaussian09 program. The optimized geometry is summarized in Table 1. From the table, the C—C bond length of C_3—C_4 (1.4183 Å) is greater than that of C_4—C_5 (1.3954 Å) and C_2—C_3 (1.3981 Å), because of the delocalization of electron density of C_3—C_4 with the ring III and with the nitro group. Also C_4—O_{10}, C_{12}—O_{10}, C_3—N_{11} and C_{12}—N_{11} bond lengths are different because of the difference in their environment, also assumes a double bond character in C_{12}—N_{11}. The bond angle between C_{13}—C_{12}—O_{10} (116.9°) and C_{13}—C_{12}—N_{11} (129.4°) indicates the π bond character of the former. Also C_4—O_{10}—C_{12} (104.3°) and C_3—N_{11}—C12 (105.8°) indicates slightly higher electronegative property of oxygen atom. The large difference between the bond lengths of C_{12}—C_{13} and C_{13}—C_{16} are because of the polarity difference of the attaching groups. The C—N bond length of C_3—N_{11}, C_1—N_{29} and C_{23}—N_{26} is only because of the greater delocalization in the nitro benzene entity.

Bond angles of C_5—C_4—O_{10} and C_2—C_3—N_{11} are higher than 120° indicates the presence of hyper-conjugative interaction. The broadening of C_4—C_5—H_8 and C_3—C_2—H_7 bond angles than that of other C—C—H bond angles also indicates the delocalization of charge in the III ring. The reduced bond angles of C_{21}—C_{23}—N_{26}, C_{19}—C_{23}—N_{26} and H_{25}—C_{21}—C_{23}, H_{24}—C_{19}—C_{23} indicating the higher electronegative property of nitro group. This also came true in the case of C_6—C1—N_{29} and C_2—C_1—N_{29} bond angles.

The substitution of nitro group in the phenyl ring increases the C—C bond lengths C_{21}—C_{23} and C_{23}—C_{19} of the benzene ring from the rest in PhII and C_1—C_6 and C_1—C_2 in PhI. Nitro group is highly electronegative and tries to obtain additional electron density of the benzene ring. It attempts to draw it from the neighboring atoms, which move closer together, in order to share the remaining electrons more easily as a result. Due to this the bond angle, A(21,23,19) is found to be 122.0°, and A(2,1,6) is found to be 123.7° in the present calculation, which is 120° for normal benzene. The bond lengths are, C_{21}—C_{23} = 1.4045 Å, C_{23}—C_{19} = 1.4064 Å for PhII and C_1—C_6 = 1.4171 Å, C_1—C_2 = 1.4058 Å for PhI, which was 1.3864 Å for benzene. Also the higher bond length C_3—C_4 (1.4183 Å) reveals the delocalization of π electrons in the ortho ring of benzene. For the title compound the bond lengths C_4—O_{10}, C_3—N_{11} are found to be 1.398 and 1.42 Å while for 2-mercaptobenzoxazole [43] these are, respectively, 1.3436 and 1.3739 Å. The bond lengths N_{11}—C_{12}, O_{10}—C_{12}, C_4—C_3 are found to increase to 1.3097, 1.4297 and 1.4183 Å from the values 1.3001, 1.3804 and 1.3927 Å obtained for 2-mercaptobenzoxazole [43]. These changes in bond lengths for the title compound can be attributed to the conjugation of the phenyl ring and the presence of a CH_2 group in the neighboring position.

The aromatic ring of the title compound is somewhat irregular and the spread of CC bond distance is 1.3954–1.4183 Å in PhI and 1.4016–1.4137 Å in PhII, which is similar to the spread reported by Smith et al. [58]. CH bond lengths in rings I and II of the title compound lie respectively, between 1.0829–1.0838 Å and 1.0842–1.0872 Å.

Chambers et al. [59] reported the N—O bond lengths in the range 1.2201–1.2441 Å, C—N length as 1.4544 Å. The experimental values of N—O bond lengths are 1.222–1.226 Å and C—N lengths in the range 1.442–1.460 Å [60]. Sundaraganesan et al. [61] reported C—N bond lengths as 1.453, 1.460 Å (SDD) and N—O bond lengths in the range 1.2728–1.2748 Å. For the title compound, the C—N bond lengths are 1.4789, 1.4775 Å and N—O bond lengths are in the range 1.2786–1.2794 Å, which are in agreement with the reported values. The CNO angles are reported [61] in the range 117.4–118.7°, where as for the title compound it is 118.1°. Purkayastha and Chattopadhyay [62] reported N_{11}=C_{12}, N_{11}—C_3 bond lengths as 1.3270, 1.400 Å for benzothiazole and 1.3503, 1.407 Å for benzimidazole compounds. Ambujakshan et al. has reported the same as 1.2753 and 1.3892 Å [20]. In the present case, the respective bond lengths are 1.3081 and 1.4113 Å.

Lifshitz et al. [63] reported the bond lengths for N_{11}—C_{12}, O_{10}—C_{12}, O_{10}—C_4, C_3—C_2, C_4—C_5, C_3—C_4, and N_{11}—C_3 as 1.291, 1.372, 1.374, 1.39, 1.4, 1.403 and 1.401 Å. The corresponding values in the present case are 1.3097, 1.4297, 1.398, 1.3981, 1.3954, 1.4183 and 1.42 Å. Corresponding values are reported as 1.2753, 1.3492, 1.359, 1.3768, 1.3879, 1.3784, 1.3892 Å [20] and 1.2727, 1.347, 1.3594, 1.3884, 1.3777, 1.3776, 1.3903 Å [19]. The corresponding reported values are 1.27, 1.3456, 1.3566, 1.3872, 1.37, 1.3854 and 1.3827 Å [64]. The bond lengths C_4—O_{10}, C_3—N_{11}, N_{11}—C_{12}, C_{12}—O_{10} and C_3—C_4 are found to be 1.3436, 1.3739, 1.3001, 1.3804 and 1.3827 Å for mercaptobenzoxazole [43].

The bond angles of the NO_2 group of the title compound O_{30}—N_{29}—O_{31} = 123.8, O_{30}—N_{29}—C_1 = 118.1, O_{31}—N_{29}—C_1 = 118.1 and O_{27}—N_{26}—O_{28} = 123.8, O_{27}—N_{26}—C_{23} = 118.1, O_{28}—N_{26}—C_{23} = 118.1 are in agreement with the values 123.5, 118.7, and 117.9° given by Saeed et al.[65].

The benzoxazole moiety is slightly tilted from tri-substituted phenyl ring as is evident from the torsion angles, C_6—C_5—C_4—O_{10} = 179.9, C_5—C_4—O_{10}—C_{12} = −179.9, C_1—C_2—C_3—N_{11} = −180.0 and C_2—C_3—N_{11}—C_{12} = 179.9° and methylene group is more tilted from the para substituted phenyl ring as is evident from torsion angles, C_{21}—C_{18}—C_{16}—C_{13} = −179.0, C_{18}—C_{16}—C_{13}—C_{12} = −122.8, C_{19}—C_{17}—C_{16}—C_{13} = 179.0 and C_{17}—C_{16}—C_{13}—C_{12} = 58.2°. The torsion angles C_{16}—C_{13}—C_{12}—N_{11} = −100.3 and C_{16}—C_{13}—C_{12}—O_{10} = 78.0°, which shows the COC and CON groups are in different planes.

First hyperpolarizability

Nonlinear optics deals with the interaction of applied electromagnetic fields in various materials to generate new electromagnetic fields, altered in wavenumber, phase, or other physical properties [66]. Organic molecules able to manipulate photonic signals efficiently are of importance in technologies such as optical communication, optical computing, and dynamic image processing [67,68]. In this context, the dynamic first hyperpolarizability of the title compound is also calculated in the present study. The first hyperpolarizability (β_0) of this novel molecular system is calculated using SDD method, based on the finite field approach. In the presence of an applied electric field, the energy of a system is a function of the electric field. First hyperpolarizability is a third rank tensor that can be described by a $3 \times 3 \times 3$ matrix. The 27 components of the 3D matrix can be reduced to 10 components due to the Kleinman symmetry [69]. The components of β are defined as the coefficients in the Taylor series expansion of the energy in the external electric field. When the electric field is weak and homogeneous, this expansion becomes

$$E = E_0 - \sum_i \mu_i F^i - \frac{1}{2}\sum_{ij} \alpha_{ij} F^i F^j - \frac{1}{6}\sum_{ijk} \beta_{ijk} F^i F^j F^k - \frac{1}{24}\sum_{ijkl} \gamma_{ijkl} F^i F^j F^k F^l + \cdots$$

where E_0 is the energy of the unperturbed molecule, F^i is the field at the origin, μ_{ij}, α_{ij}, β_{ijk} and γ_{ijkl} are the components of dipole moment, polarizability, the first hyperpolarizabilities, and second hyperpolarizibilities, respectively. The calculated first hyperpolarizability of the title compound is 8.47×10^{-30} esu, which comparable with the reported values of similar derivatives [70] and which is 65.15 times that of the standard NLO material urea (0.13×10^{-30} esu) [71]. We conclude that the title compound is an attractive object for future studies of nonlinear optical properties.

Table 3
Second-order perturbation theory analysis of Fock matrix in NBO basis corresponding to the intramolecular bonds of the title compound.

Donor (*i*)	Type	ED/e	Acceptor (*j*)	Type	ED/e	$E(2)$[a] (kcal mol^{-1})	$E(j)$–$E(i)$[b] (a.u.)	$F(i,j)$[c] (a.u.)
C1—C26	σ	1.97	C1—C6	σ*	0.02	2.91	1.21	0.053
–	–	–	C3—N11	–	0.03	6.39	1.09	0.075
–	–	–	C6—H9	–	0.01	2.28	1.23	0.048
–	–	–	N29—O31	–	0.06	2.97	1.02	0.05
C1—C2	π	1.66	C3—C4	π*	0.45	19.15	0.26	0.07
–	–	–	C5—C6	–	0.29	21.84	0.29	0.07
–	–	–	N29—O30	–	0.66	30.51	0.12	0.06
C1—C6	σ	1.98	C1—C2	σ*	0.02	2.93	1.22	0.05
–	–	–	C2—H7	–	0.01	2.57	1.22	0.05
–	–	–	C5—H8	–	0.01	2.93	1.21	0.05
–	–	–	N29—O30	–	0.06	2.91	1.02	0.05
C1—N29	σ	1.99	C2—C3	σ*	0.02	2.22	1.34	0.05
–	–	–	C5—C6	–	0.01	2.23	1.34	0.05
C2—C3	σ	1.97	C1—N29	σ*	0.10	5.23	0.97	
–	–	–	C3—C4	–	0.05	2.24	1.20	0.05
–	–	–	C4—O10	–	0.03	2.06	0.98	0.04
–	–	–	N11—C12	–	0.02	2.14	1.22	0.05
C2—H7	σ	1.97	C1—C6	σ*	0.02	5.73	1.03	0.07
–	–	–	C3—C4	–	0.05	5.31	1.01	0.07
C3—C4	σ	1.98	C2—C3	σ*	0.02	2.73	1.24	0.05
–	–	–	C2—H7	–	0.01	3.14	1.22	0.06
–	–	–	C4—C5	–	0.02	3.11	1.24	0.06
–	–	–	C5—H8	–	0.01	3.06	1.21	0.05
–	–	–	C12—C13	–	0.03	2.11	1.09	0.04
C3–C4	π	1.60	C1—C2	π*	0.36	22.93	0.29	0.07
–	–	–	C5—C6	–	0.29	17.68	0.30	0.07
–	–	–	N11—C12	–	0.24	10.71	0.27	0.05
C3—N11	σ	1.97	C4—C5	σ*	0.02	3.80	1.29	0.06
–	–	–	C12—C13	–	0.03	7.92	1.14	0.09
C4—C5	σ	1.98	C3—C4	σ*	0.05	2.56	1.21	0.05
–	–	–	C6—H9		0.01	3.07	1.25	0.06
–	–	–	O10—C12	–	0.09	2.52	0.95	0.04
C4—O10	σ	1.98	C2—C3	σ*	0.02	3.21	1.43	0.06
–	–	–	C12—C13	–	0.03	3.28	1.27	0.06
C5—C6	σ	1.97	C1—N29	σ*	0.10	4.61	0.96	0.06
–	–	–	C4—O10	–	0.03	7.30	0.97	0.08
C5—C6	π	1.67	C1—C2	π*	0.36	19.54	0.28	0.07
–	–	–	C3—C4	–	0.45	24.82	0.27	0.08
C5—H8	σ	1.98	C1—C6	σ*	0.02	4.96	1.03	0.06
–	–	–	C3—C4	–	0.05	5.33	1.01	0.07
C6—H9	σ	1.97	C1—C2	σ*	0.02	5.98	1.04	0.07
–	–	–	C4—C5	–	0.02	4.62	1.05	0.06
O10—C12	σ	1.98	C4—C5	σ*	0.02	4.79	1.39	0.07
N11—C12	σ	1.98	C2—C3	σ*	0.02	5.30	1.42	0.08
N11—C12	π	1.89	C3—C4	π*	0.02	14.35	34.00	0.07
–	–	–	C13—C16	σ*	0.03	2.87	0.70	0.04
C12—C13	σ	1.97	C3—N11	σ*	0.03	4.12	1.05	0.06
–	–	–	C4—O10	–	0.03	2.72	0.93	0.05
–	–	–	C16—C18	–	0.02	2.19	1.20	0.05
C13—H14	σ	1.96	O10—C12	σ*	0.09	7.23	0.72	0.07
–	–	–	C16—C18	–	0.02	2.06	1.04	0.04
–	–	–	C16—C18	π*	0.33	3.70	0.53	0.04
C13—H15	σ	1.97	N11—C12	σ*	0.02	4.26	1.01	0.06
–	–	–	N11—C12	π*	0.24	3.08	0.50	0.04
–	–	–	C16—C17	–	0.03	5.12	1.04	0.07
C13—C16	σ	1.96	N11—C12	σ*	0.24	3.76	0.61	0.05
–	–	–	C17—C19	π*	0.01	3.39	1.17	0.06
–	–	–	C18—C21	–	0.01	3.31	1.16	0.06
C16—C17	σ	1.97	C16—C18	σ*	0.02	2.29	1.23	0.05
–	–	–	C18—H22	–	0.02	3.03	1.20	0.05
–	–	–	C19—H24	–	0.01	2.84	1.21	0.05
C16—C18	σ	1.98	C16—C17	σ*	0.03	2.29	1.22	0.05
–	–	–	C17—H20	–	0.02	2.92	1.21	0.05
–	–	–	C21—H25	–	0.01	2.78	1.21	0.05
C16—C18	π	1.63	C12—C13	σ*	0.03	2.65	0.63	0.04
–	–	–	C13—H14	–	0.01	2.85	0.71	0.04
–	–	–	C17—C19	π*	0.28	18.09	0.28	0.07
–	–	–	C21—C23	–	0.38	24.96	0.27	0.07
C17—C19	σ	1.97	C13—C16	σ*	0.03	4.46	1.06	0.06
–	–	–	C16—C17	–	0.03	2.04	1.22	0.05
–	–	–	C23—N26	–	0.10	5.20	0.96	0.06
C17—C19	π	1.65	C16—C18	π*	0.33	23.45	0.28	0.07
–	–	–	C21—C23	–	0.38	21.02	0.27	0.07

Table 3 (*continued*)

Donor (*i*)	Type	ED/e	Acceptor (*j*)	Type	ED/e	$E(2)$[a] (kcal mol^{-1})	$E(j)$–$E(i)$[b] (a.u.)	$F(i,j)$[c] (a.u.)
C17—H20	σ	1.98	C16–C18	σ*	0.02	5.79	1.05	0.07
–	–	–	C19—C23	–	0.02	4.97	1.03	0.64
C18—C21	σ	1.97	C13—C16	σ*	0.03	4.50	1.06	0.06
–	–	–	C23—N26	–	0.10	5.24	0.95	0.06
C18—H22	σ	1.98	C16—C17	σ*	0.03	5.85	1.04	0.07
–	–	–	C21—C23	–	0.02	4.89	1.04	0.06
C19—C23	σ	1.98	C17—H20	σ*	0.02	3.05	1.22	0.06
–	–	–	C21—C23	–	0.02	3.23	1.23	0.06
–	–	–	C21—H25	–	0.01	2.65	1.22	0.05
–	–	–	N26—O28	–	0.06	2.91	1.02	0.05
C19—H24	σ	1.97	C16—C17	σ*	0.03	5.16	1.04	0.07
–	–	–	C21—C23	–	0.02	5.74	1.04	0.07
C21—C23	σ	1.98	C18—H22	σ*	0.02	3.05	1.21	0.05
–	–	–	C19—C23	–	0.02	3.23	1.23	0.06
–	–	–	C19—H24	–	0.01	2.63	1.23	0.05
–	–	–	N26—O27	–	0.06	2.91	1.02	0.05
C21—C23	π	1.64	C16—C18	π*	0.33	17.89	0.29	0.07
–	–	–	C17—C19	–	0.28	21.25	0.30	0.07
–	–	–	N26—O27	–	0.66	35.68	0.12	0.063
C21—H25	σ	1.97	C16—C18	σ*	0.02	5.11	1.05	0.07
–	–	–	C19—C23	–	0.02	5.76	1.04	0.07
C23—N26	σ	1.99	C17—C19	σ*	0.01	2.16	1.35	0.05
–		–	C18—C21	–	0.01	2.18	1.34	0.05
N26—O27	π	1.98	C21—C23	π*	0.38	4.88	0.44	0.05
–	–	–	N26—O27	–	0.66	8.47	0.27	0.05
N29—O30	π	1.98	C1—C2	π*	0.36	3.80	0.44	0.04
–		–	N29—O30	–	0.66	8.57	0.27	0.05
LP (1) O10	σ	1.97	C3—C4	σ*	0.05	3.90	1.08	0.06
–	–	–	N11—C12	–	0.02	4.11	1.10	0.06
LP (2) O10	n	1.74	C3—C4	σ*	0.45	23.56	0.35	0.09
–	–	–	N11—C12	–	0.24	29.10	0.33	0.09
LP (1) N11	σ	1.91	C3—C4	σ*	0.05	6.81	0.84	0.07
–	–	–	O10—C12	–	0.09	15.75	0.58	0.09
–	–	–	C12—C13	–	0.03	0.53	0.75	0.02
LP (1) O27	σ	1.98	C23—N26	σ*	0.10	5.37	1.06	0.07
–	–	–	N26—O28	–	0.06	2.22	1.11	0.05
LP (2) O27	n	1.91	C23—N26	σ*	0.10	10.34	0.54	0.07
–	–	–	N26—O28	–	0.10164	18.15	0.59	0.09
LP (1) O28	σ	1.977	C23—N26	σ*	0.10	5.37	1.06	0.069
–	–	–	N26—O27	–	0.05938	2.22	1.11	0.05
LP(2) O28	σ	1.912	C23—N26	σ*	0.10	10.33	0.54	0.067
–	–	–	N26—O27	–	0.05938	18.12	0.59	0.093
LP(3) O28	–	1.435	N26—O27	π*		0.65952	168.07	0.125
LP(1) O30	σ	1.9774	C1—N29	σ*	0.02482	5.38	1.06	0.069
–	–	–	N29—O31	–	0.05917	2.22	1.11	0.045
LP(2) O30	π	1.9116	C1—N29	σ*	0.02482	10.56	0.53	0.067
–	–	–	N29—O31	–	0.05917	18.1	0.59	0.093
LP(1) O31	σ	1.9775	C1—N29	σ*	0.02482	5.37	1.06	0.069
–	–	–	N29—O30	–	0.05893	2.24	1.11	0.045
LP(2) O31	π	1.9118	C1—N29	σ*	0.02482	10.52	0.53	0.067
–	–	–	C1—N29	–	0.05893	18.03	0.59	0.093
LP(3)O31	n	1.4359	C1—N29	π*	0.66031	168.16	0.11	0.125

[a] $E(2)$ means energy of hyper-conjugative interactions (stabilization energy).
[b] Energy difference between donor and acceptor i and j NBO orbitals.
[c] $F(i,j)$ if the Fock matrix element between i and j NBO orbitals.

NBO analysis

The natural bond orbitals (NBOs) calculations were performed using NBO 3.1 program [72] as implemented in the Gaussian09 package at the DFT/B3LYP level in order to understand various second-order interactions between the filled orbitals of one subsystem and vacant orbitals of another subsystem, which is a measure of the intermolecular delocalization or hyper-conjugation. NBO analysis provides the most accurate possible 'natural Lewis structure' picture of 'j' because all orbital details are mathematically chosen to include the highest possible percentage of the electron density. A useful aspect of the NBO method is that it gives information about interactions of both filled and virtual orbital spaces that could enhance the analysis of intra and inter molecular interactions.

The second-order Fock-matrix was carried out to evaluate the donor–acceptor interactions in the NBO basis. The interactions result in a loss of occupancy from the localized NBO of the idealized Lewis structure into an empty non-Lewis orbital. For each donor (i) and acceptor (j) the stabilization energy (E2) associated with the delocalization $i \rightarrow j$ is determined as

$$E(2) = \Delta E_{ij} = q_i \frac{(F_{i,j})^2}{(E_j - E_i)}$$

where $q_i \rightarrow$ donor orbital occupancy, E_i, $E_j \rightarrow$ diagonal elements, $F_{ij} \rightarrow$ the off diagonal NBO Fock matrix element.

In NBO analysis large $E(2)$ value shows the intensive interaction between electron-donors and electron-acceptors, and greater the extent of conjugation of the whole system, the possible intensive

Table 4
NBO results showing the formation of Lewis and non-Lewis orbitals.

Bond (A—B)	ED/energy (a.u.)	EDA%	EDB%	NBO	s%	p%
σ C1—C2	1.97193	50.51	49.49	$0.7107(sp^{1.64})C$	37.92	62.08
–	−0.75010	–	–	$+0.7035(sp^{1.93})C$	34.18	65.82
π C1—C2	1.65792	55.94	44.06	$0.7480(sp^{1.00})C$	0.0	100
–	−0.30738	–	–	$+0.6637(sp^{1.00})C$	0.0	100
σ C1—C6	1.9758	50.96	49.04	$0.7139(sp^{1.64})C$	37.86	62.14
–	−0.74602	–	–	$+0.7003(sp^{1.92})C$	34.29	65.71
σ C1—N29	1.98643	36.69	63.31	$0.6057(sp^{3.15})C$	24.09	75.91
–	−0.84037	–	–	$+0.7957(sp^{1.70})N$	37.02	62.98
σ C2—C3	1.97213	49.4	50.6	$0.7029(sp^{1.85})C$	35.08	64.92
–	−0.75281	–	–	$+0.7113(sp^{1.58})C$	38.83	61.17
σ C3—C4	1.97562	49.83	50.17	$0.7059(sp^{2.09})C$	32.34	67.66
–	−0.74346	–	–	$+0.7083(sp^{1.85})C$	35.05	64.95
π C3—C4	1.59765	51.8	48.2	$0.7197(sp^{1.00})C$	0	100
–	−0.31234	–	–	$+0.6943(sp^{1.00})C$	0	100
σ C3—N11	1.96765	40.89	59.11			
–	−0.79784	–	–	$+0.7689(sp^{2.34})N$	29.94	70.06
σ C4—C5	1.977	50.85	49.15	$0.7131(sp^{1.45})C$	40.87	59.13
–	−0.76422	–	–	$+0.7010(sp^{1.94})C$	34.03	65.97
σ C4—O10	1.98472	31.09	68.91	$0.5576(sp^{3.18})C$	23.92	76.08
–	−0.92583	–	–	$+0.8301(sp^{2.38})O$	29.60	70.4
σ C5—C6	1.96941	50.2	49.8	$0.7086(sp^{1.82})C$	35.4	64.6
–	−0.73821	–	–	$+0.7057(sp^{1.80})C$	35.72	64.28
π C5—C6	1.67339	51.88	48.12	$0.7203(sp^{1.00})C$	0	100
–	−0.29919	–	–	$+0.6937(sp^{1.00})C$		–
σ O10—C12	1.98454	70.5	29.5	$0.8396(sp^{2.64})O$	27.47	72.53
–	−0.89383	–	–	$+0.5432(sp^{3.09})C$	24.45	75.55
σ N11—C12	1.98207	60.33	39.67	$0.7768(sp^{1.79})N$	35.85	64.15
–	−0.92107	–	–	$+0.6298(sp^{1.80})C$	35.70	64.3
π N11—C12	1.89409	59.01	40.99	$0.7682(sp^{1.00})C$	0	100
–	−0.37078	–	–	$+0.6402(sp^{1.00})C$	0	100
σ C12—C13	1.96655	49.96	50.04	$0.7068(sp^{1.51})C$	39.83	60.17
–	−0.70608	–	–	$+0.7074(sp^{2.76})C$	26.58	73.42
σ C13—C16	1.95929	50.76	49.24	$0.7124(sp^{2.47})C$	28.81	71.19
–	−0.65851	–	–	$+0.7017(sp^{2.26})C$	30.70	69.3
σ C16—C17	1.97487	50.41	49.59	$0.7100(sp^{1.90})C$	34.47	65.53
–	−0.72816	–	–	$+0.7042(sp^{1.80})C$	35.66	64.34
σ C16—C18	1.975	50.42	49.58	$0.7101(sp^{1.87})C$	34.89	65.17
–	−0.73139	–	–	$+0.7041(sp^{1.77})C$	36.04	63.96
π C16—C18	1.63283	49.26	50.74	$0.7019(sp^{1.00})C$	0	100
–	−0.28887	–	–	$+0.7123(sp^{1.00})C$	0	100
σ C17—C19	1.97332	49.85	50.15	$0.7060(sp^{1.85})C$	35.14	64.86
–	−0.72926	–	–	$+0.7082(sp^{1.78})C$	35.95	64.05
π C17—C19	1.64514	51.65	48.35	$0.7186(sp^{1.00})C$	0	100
–	−0.28876	–	–	$+0.6954(sp^{1.00})C$	0	100
σ C18—C21	1.97304	49.85	50.15	$0.7060(sp^{1.86})C$	34.97	65.03
–	−0.72855	–	–	$+0.7082(sp^{1.79})C$	35.84	64.16
σ C19—C23	1.97555	49.05	50.95	$0.7004(sp^{1.93})C$	34.08	65.92
–	−0.74241	–	–	$+0.7138(sp^{1.64})C$	37.87	62.13
σ C21—C23	1.97554	49.1	50.9	$0.7007(sp^{1.92})C$	34.19	65.81
–	−0.74407	–	–	$+0.7135(sp^{1.64})C$	37.88	62.12
π C21—C23	1.63796	44.76	55.24	$0.6690(sp^{1.00})C$	0	100
–	−0.30006	–	–	$+0.7432(sp^{1.00})C$	0	100
σ C23—N26	1.98703	36.61	63.39	$0.6051(sp^{3.14})C$	24.14	75.86
–	−0.83734	–	–	$+0.7962(sp^{1.69})C$	37.14	62.86
σ N26—O27	1.99149	49.4	50.6	$0.7029(sp^{2.20})C$	31.29	68.71
–	−1.03475	–	–	$+0.7113(sp^{4.14})C$	19.45	80.55
π N26—O27	1.9831	41.49	58.51	$0.6441(sp^{1.00})C$	0	100
–	−0.45709	–	–	$+0.7649(sp^{1.00})C$	0	100
σ N26—O28	1.99148	49.4	50.6	$0.7029(sp^{2.20})C$	31.28	68.72
–	−1.03437	–	–	$+0.7113(sp^{4.14})C$	19.44	80.56
σ N29—O30	1.99141	49.44	50.56	$0.7031(sp^{2.19})C$	31.35	68.65
–	−1.03853	–	–	$+0.7111(sp^{4.14})C$	19.44	80.56
π N29—O30	1.98383	41.51	58.49	$0.6443(sp^{1.00})C$	0	100
–	−0.4603	–	–	$+0.7648(sp^{1.00})C$	0	100
σ N29—O31	1.9914	49.43	50.57	$0.7031(sp^{2.19})C$	31.33	68.67
–	−1.03815	–	–	$+0.7111(sp^{4.14})C$	19.43	57.07
n1 O10	1.97303	–	–	$sp^{2.19}$	42.93	57.07
–	−0.63212	–	–	–	–	–
n2 O10	1.73925	–	–	$sp^{1.00}$	0	100
–	−0.37847	–	–	–	–	–
n1 N11	1.90769		–	$sp^{1.92}$	34.23	65.77
–	−0.39988	–	–	–	–	–
n1 O27	1.97769		–	$sp^{0.24}$	80.42	19.58
–	−0.83235	–	–	–	–	–

Table 4 (*continued*)

Bond (A—B)	ED/energy (a.u.)	EDA%	EDB%	NBO	s%	p%
n2 O27	1.91239	–	–	$sp^{99.99}$	0.2	99.8
–	−0.31149	–	–	–	–	–
n1 O28	1.9777	–	–	$-sp^{0.24}$	80.42	19.58
–	−0.83240	–	–	–		–
n2 O28	1.91244	–	–	$sp^{99.99}$	0.2	99.8
–	−0.31148	–	–	–	–	–
n3 O28	1.43588	–	–	$sp^{1.00}$	0	100
–	−0.29331	–	–	–	–	–
n1 O30	1.9774	–	–	$-sp^{0.24}$	80.45	19.55
–	−0.83540	–	–	–	–	–
n2 O30	1.91163	–	–	$sp^{99.99}$	0.17	99.83
–	−0.31421	–	–	–	–	–
n1 O31	1.97751	–	–	$sp^{0.24}$	80.46	19.54
–	−0.83568	–	–	–	–	–
n2 O31	1.91186	–	–	$sp^{99.99}$	0.18	99.82
–	0.31450	–	–	–	–	–
n3 O31	1.43592	–	–	$sp^{1.00}$	0	100
–	−0.29637	–	–	–		–

interaction are given in NBO Table 3. The second-order perturbation theory analysis of Fock-matrix in NBO basis shows strong intermolecular hyper-conjugative interactions are formed by orbital overlap between n(O) and π^* (N—O), π^* (N—C) bond orbitals which result in ICT causing stabilization of the system. These interactions are observed as an increase in electron density (ED) in N—O and N—C anti bonding orbital that weakens the respective bonds. There occurs a strong inter molecular hyper-conjugative interaction in N_{26}—O_{27} from O_{28} of $n_3(O_{28}) \rightarrow \pi^*$ (N_{26}—O_{27}) which increases ED (0.65952e) that weakens the respective bonds leading to stabilization of 168.07 kcal mol^{-1} and also the hyper-conjugative interaction in O_{10} of $n_2(O_{10}) \rightarrow \pi^*$ (N_{11}—C_{12}) which increases ED (0.24 e) that weakens the respective bonds N_{11}—C_{12} leading to stabilization of 29.10 kJ/mol. An another hyper-conjugative interaction observed in C_1—N_{29} from O31 of $n_3(O_{31}) \rightarrow \pi^*$ (C_1—N_{29}) which increases ED (0.66031e) that weakens the respective bonds leading to stabilization of 168.16 kcal mol^{-1}. These interactions are observed as an increase in electron density (ED) in N—O and N—C anti bonding orbitals that weakens the respective bonds.

The increased electron density at the oxygen atoms leads to the elongation of respective bond length and a lowering of the corresponding stretching wave number. The electron density (ED) is transferred from the n (O) to the anti-bonding π^* orbital of the N—O and N—C bonds, explaining both the elongation and the red shift [73]. The hyper-conjugative interaction energy was deduced from the second-order perturbation approach. Delocalization of electron density between occupied Lewis-type (bond or lone pair) NBO orbitals and formally unoccupied (anti bond or Rydberg) non-Lewis NBO orbitals corresponds to a stabilizing donor–acceptor interaction. The C═N and NO_2 stretching modes can be used as a good probe for evaluating the bonding configuration around the N atoms and the electronic distribution of the benzene molecule. Hence the 5-nitro-(2-*p*-nitrobenzyl) benzoxazole structure is stabilized by these orbital interactions.

The NBO analysis also describes the bonding in terms of the natural hybrid orbital $n_2(O_{27})$, which occupy a higher energy orbital (−0.31149 a.u.) with considerable p-character (99.80%) and low occupation number (1.91239 a.u.) and the other $n_1(O_{27})$ occupy a lower energy orbital (−0.83235 a.u.) with p-character (19.58%) and high occupation number (1.97769 a.u.). Also for the natural hybrid orbital $n_2(O_{30})$, which occupy a higher energy orbital (−0.31421 a.u.) with considerable p-character (99.83%) and low occupation number (1.91163 a.u.) and the other $n_1(O_{30})$ occupy a lower energy orbital (−0.83540 a.u.) with p-character (19.55%) and high occupation number (1.9774 a.u.) Thus, a very close to pure p-type lone pair orbital participates in the electron donation to the π^* (N—O) orbital for $n_2(O) \rightarrow \sigma^*$ (N—O) interaction in the compound. The results are tabulated in Table 4.

Mulliken charges

The calculation of atomic charges plays an important role in the application of quantum mechanical calculations to molecular

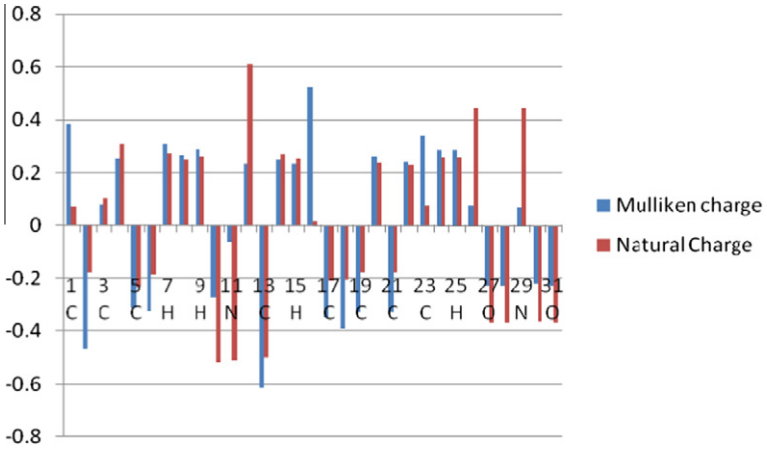

Fig. 4. Mullicken's plot.

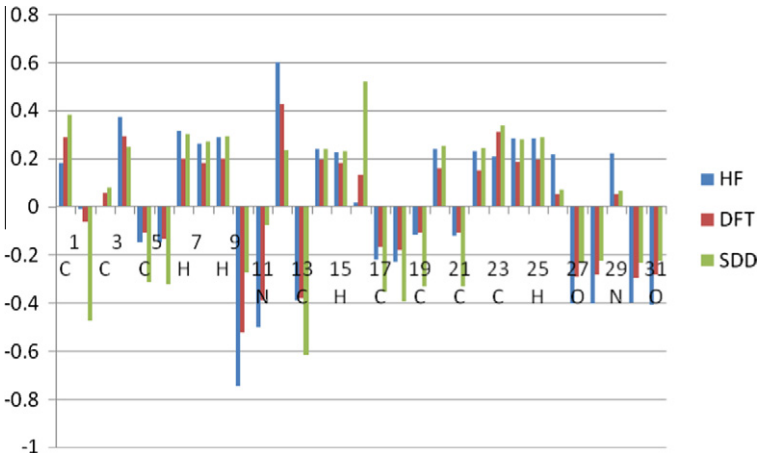

Fig. 5. Comparison of different methods for calculated atomic charges of 5-nitro-2-(4-nitrobenzyl) benzoxazole.

systems. Mulliken charges are calculated by determining the electron population of each atom as defined in the basis functions. The charge distributions calculated by the Mulliken [74] and NBO methods for the equilibrium geometry of 5-nitro-(2-*p*-nitrobenzyl) benzoxazole are given in Table S1 (Supplementary material). The charge distribution on the molecule has an important influence on the vibrational spectra. In 5-nitro-(2-*p*-nitrobenzyl) benzoxazole the Mulliken atomic charge of the carbon atoms in the neighborhood of C_1, C_4, C_{16} and C_{23} become more positive, shows the direction of delocalization and shows that the natural atomic charges are more sensitive to the changes in the molecular structure than Mulliken's net charges. The results are represented in Fig. 4.

Also we done a comparison of Mullicken charges obtained by different basic sets and tabulated in Table S2 (Supplementary material) in order to assess the sensitivity of the calculated charges to changes in (i) the choice of the basis set; (ii) the choice of the quantum mechanical method. The results can, however, better be represented in graphical form as shown in Fig. 5. We have observed a change in the charge distribution by changing different basis sets.

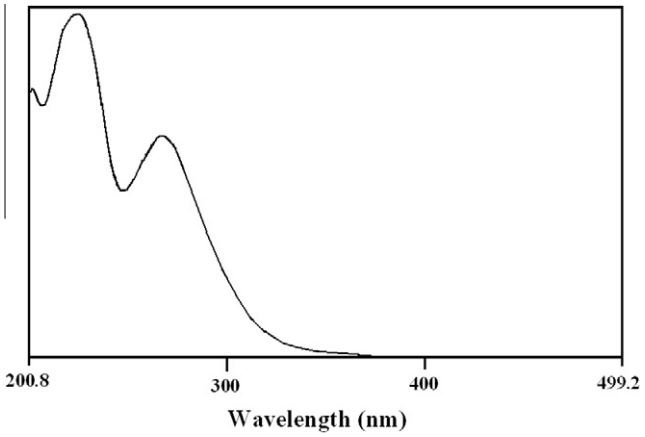

Fig. 6. UV–Vis spectrum of 5-nitro-2-(4-nitrobenzyl) benzoxazole.

Electronic absorption spectra

Electronic transitions are usually classified according to the orbitals engaged or to specific parts of the molecule involved. Common types of electronic transitions in organic compounds are π–π^*, n–π^* and π^*(acceptor)–π(donor). The UV–Vis bands in 5-nitro-2-(4-nitrobenzyl) benzoxazole are observed at 268, 225, and 208 nm (experimental values). Observed band at 208 nm is due to the π–π^*. The less intense band centered at 225 nm is due to the partly forbidden n–π^* transition from HOMO to LUMO. The more intense band observed at 268 nm belonged to the dipole-allowed π–π^* transition. The UV–Vis spectrum is shown in Fig. 6.

In order to understand the electronic transitions of 5-nitro-(2-*p*-nitrobenzyl) benzoxazole, TD-DFT calculation on electronic absorption spectrum in vacuum was performed. TD-DFT calculation is capable of describing the spectral features of 5-nitro-2-(4-

Table 5
Calculated electronic absorption spectrum of 5-nitro-2-(4-nitrobenzyl) benzoxazole using TD-DFT/B3LYP/SDD.

Excitation	CI expansion coefficient	Energy (eV)	Wavelength calc. (nm)	Wavelength exp. (nm)	Oscillator strength (*f*)
Excited state					
1					
68 → 78	0.60239	3.4644	357.88	268	0.0022
68 → 79	−0.12871				
77 → 78	−0.12856				
2					
68 → 78	0.12191	3.5082	353.41	225	0.0307
76 → 79	0.14111				
76 → 80	0.13651				
77 → 78	0.31196				
77 → 79	0.51586				
3					
77 → 78	0.57383	3.8102	325.40	208	0.0271
77 → 79	−0.33086				

nitrobenzyl) benzoxazole because of the qualitative agreement of line shape and relative strength as compared with experiment. The absorption spectra of organic compounds stem from the ground-to-excited state vibrational transition of electrons. The intense band in the UV range of the electronic absorption spectrum is observed at 268 nm, which is indicating the presence of chromophoric NO_2 in the ring. The calculated three lowest-energy transitions of the molecule from TD-DFT method and the observed electronic transitions are listed in Table 5. From the table the calculated energy transitions are red shifted from the experimental value, because these bands are observed in gas phase without considering the solvent effect.

^{1}H NMR spectrum

The experimental spectrum data of 5-nitro-2-(4-nitrobenzyl) benzoxazole in DMSO with TMS as internal standard is obtained at 400 MHz and is displayed in Table 6. The absolute isotropic chemical shielding of 5-nitro-(2-*p*-nitrobenzyl) benzoxazole was calculated by B3LYP/GIAO model [75]. Relative chemical shifts were then estimated by using the corresponding TMS shielding: σ_{calc} (TMS) calculated in advance at the same theoretical level as this paper. Numerical values of chemical shift $\delta_{pred} = \sigma_{calc}$ (TMS) $- \sigma_{calc}$ together with calculated values of σ_{calc} (TMS), are reported in Table 6. It could be seen from Table 6 that chemical shift was in agreement with the experimental ^{1}H NMR data. Thus, the results showed that the predicted proton chemical shifts were in good agreement with the experimental data for 5-nitro-(2-*p*-nitrobenzyl) benzoxazole.

Table 6
Experimental and calculated ^{1}H NMR parameters (with respect to TMS).

Proton	σ_{TMS}	B3LYP/6-31G σ_{calc}	δ_{calc} ($\sigma_{TMS} - \sigma_{calc}$)	Exp δ_{ppm}
H7	32.7711	23.7754	8.9957	8.616
H8		24.9121	7.859	7.732
H9		23.9987	8.7724	8.606
H14		28.1617	4.6094	4.650
H15		28.4950	4.2761	4.650
H20		24.8185	7.9526	7.965
H22		24.797	7.9741	7.996
H24		24.2054	8.5657	8.303
H25		24.0852	8.6859	8.331

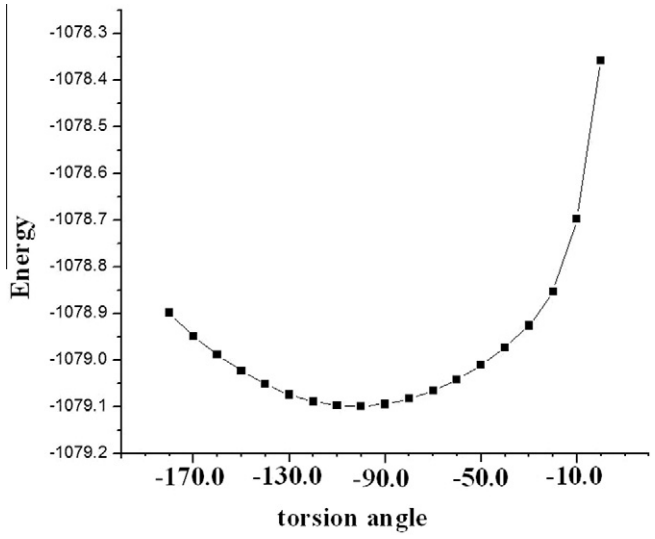

Fig. 7. Profile of potential energy scan for the torsion angle N11—C12—C13—C16.

PES scan studies

A detailed potential energy surface (PES) scan on dihedral angles N_{11}—C_{12}—C_{13}—C_{16}, C_{12}—C_{13}—C_{16}—C_{17} and C_{12}—C_{13}—C_{16}—C_{18} have been performed at B3LYP/6-31G(d) level to reveal all possible

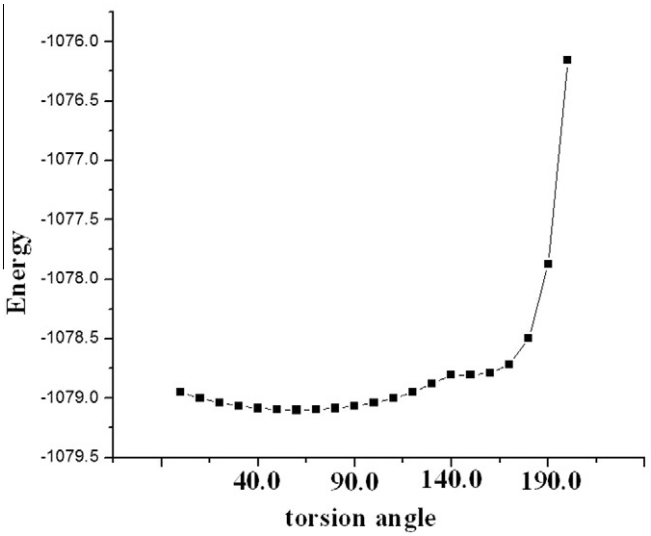

Fig. 8. Profile of potential energy scan for the torsion angle C12—C13—C16—C17.

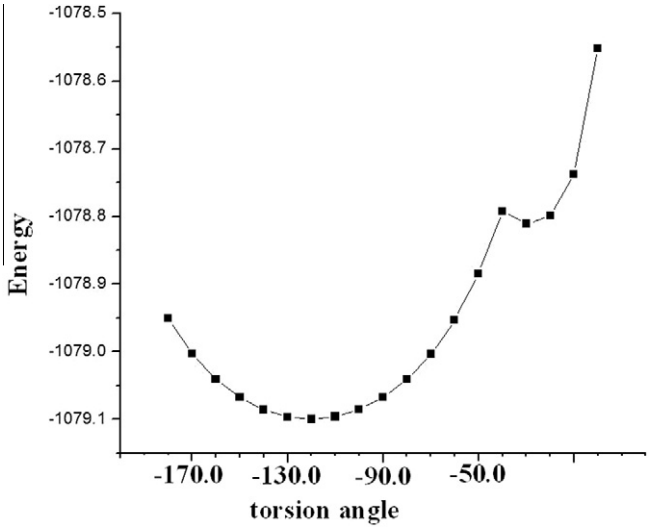

Fig. 9. Profile of potential energy scan for the torsion angle C12—C13—C16—C18.

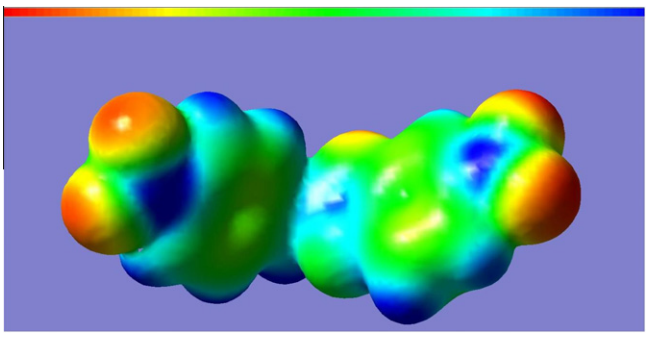

Fig. 10. Molecular electrostatic potential map calculated at B3LYP/SDD level.

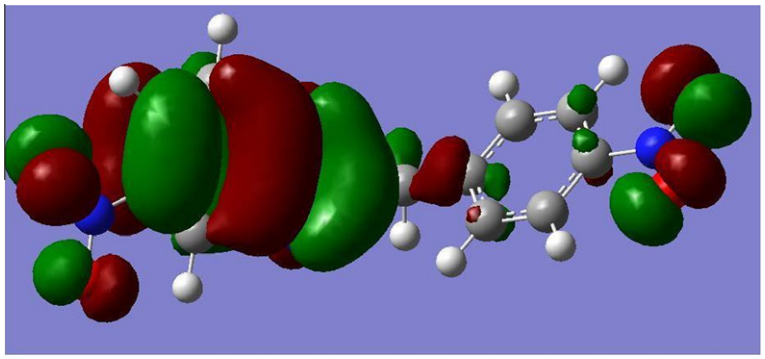

Fig. 11. HOMO plot of 5-nitro-2-(4-nitrobenzyl) benzoxazole.

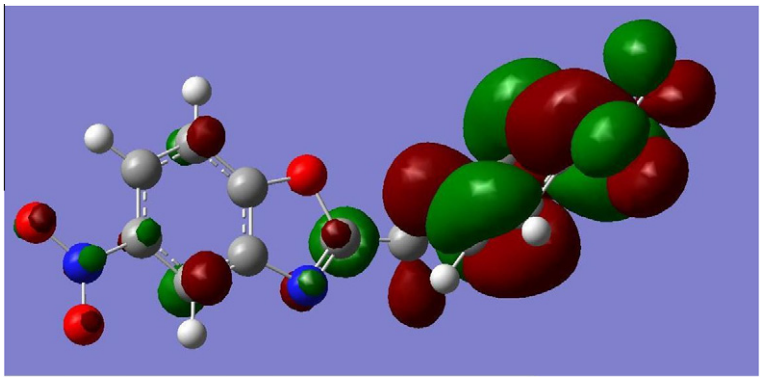

Fig. 12. LUMO plot of 5-nitro-2-(4-nitrobenzyl) benzoxazole.

conformations of 5-nitro-2-(4-nitrobenzyl) benzoxazole. The PES scan was carried out by minimizing the potential energy in all geometrical parameters by changing the torsion angle at every 10° for a 180° rotation around the bond. The results obtained in PES scan study by varying the torsional perturbation around the methyl bonds (CH_2) are plotted in Figs. 7–9. For the N_{11}—C_{12}—C_{13}—C_{16} rotation, the minimum energy was obtained at 100.3° in the potential energy curve of energy −1079.1 Hartrees. For the C_{12}—C_{13}—C_{16}—C_{17} rotation, the minimum energy occurs at 58.2° in the potential energy curve of energy −1079.1. For the C_{12}—C_{13}—C_{16}—C_{18} rotation, the minimum energy occurs at −122.2° in the potential energy curve of energy −874.33165 Hartrees.

Molecular electrostatic potential

MEP is related to the ED and is a very useful descriptor in understanding sites for electrophilic and nucleophilic reactions as well as hydrogen bonding interactions [76,77]. The electrostatic potential $V(r)$ is also well suited for analyzing processes based on the "recognition" of one molecule by another, as in drug-receptor, and enzyme–substrate interactions, because it is through their potentials that the two species first "see" each other [78,79]. To predict reactive sites of electrophilic and nucleophilic attacks for the investigated molecule, MEP at the B3LYP/6-31G(d,p) optimized geometry was calculated. The negative (red and yellow[1]) regions of MEP were related to electrophilic reactivity and the positive (blue) regions to nucleophilic reactivity (Fig. 10). From the MEP it is evident that the negative charge covers the nitro group and the positive region is over the methyl group. The more electro negativity in the nitro group makes it the most reactive part in the molecule.

HOMO–LUMO band gap

HOMO and LUMO are the very important parameters for quantum chemistry. The conjugated molecules are characterized by a highest occupied molecular orbital–lowest unoccupied molecular orbital (HOMO–LUMO) separation, which is the result of a significant degree of ICT from the end-capping electron-donor groups to the efficient electron-acceptor groups through π-conjugated path. The strong charge transfer interaction through π-conjugated bridge results in substantial ground state donor–acceptor mixing and the appearance of a charge transfer band in the electronic absorption spectrum. Therefore, an ED transfer occurs from the more aromatic part of the π-conjugated system in the electron-donor side to its electron-withdrawing part. The atomic orbital components of the frontier molecular orbitals are shown in Figs. 11 and 12. The HOMO–LUMO energy gap value is found to be 0.132 eV, which is responsible for the bioactive property of the compound 5-nitro-2-(4-nitrobenzyl) benzoxazole.

Conclusion

The geometry optimization has been carried out using HF and DFT levels. The simultaneous activation of the phenyl ring stretching modes in IR and Raman spectra are evidence for charge transfer interaction between the donor and the acceptor group through the π system. This is responsible for the bioactivity of the molecule. The NBO analysis confirms the ICT formed by the orbital overlap between n (O) and σ^* (N—O). A very close to pure p-type lone pair orbital participates in the electron donation to the σ^* (C—C) orbital

[1] For interpretation of color in Fig. 10, the reader is referred to the web version of this article.

for $n2(O_{27}) \rightarrow \sigma^*(N{-}O)$ and $n2(O_{30}) \rightarrow \sigma^*(N{-}O)$ interaction in the molecule. Overall, the TD-DFT calculations on the molecule provided deep insight into their electronic structures and properties. In addition, the calculated ^1H NMR and UV–Vis results are all in good agreement with the experimental data .The lowering of HOMO–LUMO band gap supports bioactive property of the molecule. MEP predicts the most reactive part in the molecule. The calculated first hyperpolarizability is comparable with the reported values of similar derivatives and is an attractive object for future studies of nonlinear optics.

Acknowledgment

The authors are thankful to University of Antwerp for access to University's CalcUA supercomputer cluster.

Appendix A. Supplementary material

Supplementary data associated with this article can be found, in the online version, at http://dx.doi.org/10.1016/j.saa.2012.09.032.

References

[1] A.D. Rodrıguez, C. Ramırez, I.I. Rodrıguez, E. Gonzalez, Org. Lett. 1 (1999) 527–530.
[2] M. Prudhomme, J. Guyot, G. Jeminet, J. Antibiot. 39 (1986) 934–937.
[3] S.M. Rida, F.A. Ashour, S.A.M. El-Hawash, M.M. ElSemary, M.H. Badr, M.A. Shalaby, Eur. J. Med. Chem. 40 (2005) 949–959.
[4] I. Yildiz-Oren, I. Yalcin, E. Aki-Sener, N. Ucarturk, Eur. J. Med. Chem. 39 (2004) 291–298.
[5] I. Yildiz-Oren, B. Tekiner-Gulbas, I. Yalcin, O. Temiz-Arpaci, E. Aki- Sener, N. Altanlar, Arch. Pharm. 337 (2004) 402–410.
[6] O. Temiz-Arpaci, A. Ozdemir, I. Yalcin, I. Yildiz, E. Aki-Sener, N. Altanlar, Arch. Pharm. 338 (2005) 105–111.
[7] A. Akbay, I. Oren, O. Temiz-Arpaci, E. Aki-Sener, I. Yalcin, Arzneim. Forsch. 53 (2003) 266–272.
[8] R.K. Plemper, K.J. Erlandson, A.S. Lakdawala, A. Sun, A. Prussia, J. Boonsombat, E. Aki-Sener, I. Yalcin, I. Yildiz, O. Temiz-Arpaci, B.P. Tekiner, D. Liotta, J.P. Snyder, Proc. Natl. Acad. Sci. USA 101 (2004) 5628–5634.
[9] H. Lage, E. Aki-Sener, I. Yalcin, Int. J. Cancer 119 (2006) 213–220.
[10] A. Pınar, P. Yurdakul, I. Yildiz, O. Temiz-Arpaci, N.L. Acan, E. Aki-Sener, I. Yalcin, Biochem. Biophys. Res. Commun. 317 (2004) 670–674.
[11] O. Temiz-Arpaci, B. Tekiner-Gulbas, I. Yildiz, E. Aki-Sener, I. Yalcin, Bioorg. Med. Chem. 13 (2005) 6354–6359.
[12] B. Tekiner-Gulbas, O. Temiz-Arpaci, I. Yildiz, E. Aki-Sener, I. Yalcin, SAR QSAR Environ. Res. 17 (2006) 121–132.
[13] W.D. Dunwell, D. Evans, J. Med. Chem. 20 (1977) 797–801.
[14] Farbenfabriken, A.G. Bayer, Netherlands Patent 6505511, 1965.
[15] I. Yalcin, E. Sener, S. Ozden, A. Akin, S. Yildiz, J. Pharm. Sci. 11 (1986) 257–269.
[16] E. Sener, S. Ozden, I. Yalcin, T. Ozden, A. Akin, S. Yildiz, J. Pharm. Sci. 11 (1986) 190–202.
[17] S. Ozden, T. Ozden, E. Sener, A. Akin, S. Yildiz, J. Pharm. Sci. 12 (1987) 39–47.
[18] E. Sener, I. Yalcin, S. Ozden, T. Ozden, A. Akin, S. Yildiz, J. Med. Pharm. 11 (1987) 391–396.
[19] P.L. Anto, C.Y. Panicker, H.T. Varghese, D. Philip, O. Temiz-Arpaci, B. Tekiner-Gulbas, I. Yildiz, Spectrochim. Acta 67A (2007) 744–749.
[20] K.R. Ambujakshan, V.S. Madhavan, H.T. Varghese, C.Y. Panicker, O. Temiz-Arpaci, B. Tekiner-Gulbas, I. Yildiz, Spectrochim. Acta 69A (2008) 782–788.
[21] N. Noyanalpan, E. Sener, FABAD J. Pharm. Sci. 11 (1986) 111–119.
[22] E. Sener, I. Yalcin, A. Akin, N. Noyanalpan, J. Fac. Pharm. Gazi. 4 (1987) 1–9.
[23] I. Yalcin, E. Sener, T. Ozden, S. Ozden, A. Akin, Eur. J. Med. Chem. 25 (1990) 705–708.
[24] M.J. Frisch, G.W. Trucks, H.B. Schlegel, G.E. Scuseria, M.A. Robb, J.R. Cheeseman, G. Scalmani, V. Barone, B. Mennucci, G.A. Petersson, H. Nakatsuji, M. Caricato, X. Li, H.P. Hratchian, A.F. Izmaylov, J. Bloino, G. Zheng, J.L. Sonnenberg, M. Hada, M. Ehara, K. Toyota, R. Fukuda, J. Hasegawa, M. Ishida, T. Nakajima, Y. Honda, O. Kitao, H. Nakai, T. Vreven, J.A. Montgomery, Jr., J.E. Peralta, F. Ogliaro, M. Bearpark, J.J. Heyd, E. Brothers, K.N. Kudin, V.N. Staroverov, T. Keith, R. Kobayashi, J. Normand, K. Raghavachari, A. Rendell, J.C. Burant, S.S. Iyengar, J. Tomasi, M. Cossi, N. Rega, J.M. Millam, M. Klene, J.E. Knox, J.B. Cross, V. Bakken, C. Adamo, J. Jaramillo, R. Gomperts, R.E. Stratmann, O. Yazyev, A.J. Austin, R. Cammi, C. Pomelli, J.W. Ochterski, R.L. Martin, K. Morokuma, V.G. Zakrzewski, G.A. Voth, P. Salvador, J.J. Dannenberg, S. Dapprich, A.D. Daniels, O. Farkas, J.B. Foresman, J.V. Ortiz, J. Cioslowski, D.J. Fox, Gaussian 09, Revision B.01, Gaussian, Inc., Wallingford CT, 2010.
[25] J.B. Foresman, in: E. Frisch (Ed.), Exploring Chemistry with Electronic Structure Methods: A Guide to Using Gaussian, Gaussian, Inc., Pittsburg, PA, 1996.
[26] P.J. Hay, W.R. Wadt, J. Chem. Phys. 82 (1985) 270–283.
[27] J.Y. Zhao, Y. Zhang, L.G. Zhu, J. Mol. Struct. Theochem. 671 (2004) 179–187.
[28] Roy Dennington, Todd Keith, John Millam, GaussView, Version 5, Semichem Inc., Shawnee Mission KS, 2009.
[29] J.M.L. Martin, C. Van Alsenoy, GAR2PED, A Program to Obtain a Potential Energy Distribution from a Gaussian Archive Record, University of Antwerp, Belgium, 2007.
[30] N.P.G. Roeges, A Guide to the Complete Interpretation of Infrared Spectra of Organic Structures, Wiley, New York, 1994.
[31] R.M. Silverstein, F.X. Webster, Spectrometric Identification of Organic Compounds, sixth ed., John Wiley, Asia, 2003.
[32] A. Perjessy, D. Rasala, P. Tomasik, R. Gawinecki, Collect. Czech. Chem. Commun. 50 (1985) 2443–2452.
[33] J.F. Brown Jr., J. Am. Chem. Soc. 77 (1955) 6341–6351.
[34] J.H.S. Green, W. Kynanston, A.S. Lindsey, Spectrochim. Acta 17 (1961) 486–502.
[35] O. Exner, S. Kovac, E. Solcaniova, Collect. Czech. Chem. Commun. 37 (1972) 2156–2168.
[36] G. Varsanyi, E. Molner-Pall, K. Kosa, G. Keresztury, Acta Chim. Acad. Sci. Hung. 106 (1979) 481–498.
[37] V. Suryanarayana, A.P. Kumar, G.R. Rao, G.C. Panday, Spectrochim. Acta 48A (1992) 1481–1489.
[38] R. Saxena, L.D. Kaudpal, G.N. Mathur, J. Polym. Sci. Part A: Polym. Chem. 40 (2002) 3959–3966.
[39] R.M. Silverstein, G.C. Bassler, T.C. Morril, Spectrometric Identification of Organic Compounds, 5th ed., John Wiley and Sons Inc., Singapore, 1991.
[40] K. Nakamoto, Infrared and Raman Spectrum of Inorganic and coordination Compounds, 5th ed., John Wiley and Sons, Inc., New York, 1997.
[41] T.D. Klots, W.B. Collier, Spectrochim. Acta 51A (1995) 1291–1316.
[42] N.B. Colthup, L.H. Daly, S.E. Wiberly, Introduction to Infrared and Raman Spectroscopy, 3rd ed., Academic Press, Boston, 1990.
[43] A. Bigotto, B. Pergolese, J. Raman Spectrosc. 32 (2001) 953–959.
[44] N. Sandhyarani, G. Skanth, S. Berchmanns, V. Yegnaraman, T. Pradeep, J. Colloid Interface Sci. 209 (1999) 154–161.
[45] J. Coates, in: R.A. Meyers (Ed.), Encyclopedia of Analytical Chemistry; Interpretation of Infrared Spectra. A Practical Approach, John Wiley and Sons Ltd., Chichester, 2000.
[46] P. Sett, N. Paul, S. Chattopadhyay, P.K. Mallick, J. Raman Spectrosc. 30 (1999) 277–287.
[47] P. Sett, S. Chattopadhyay, P.K. Mallick, Spectrochim. Acta 56A (2000) 855–875.
[48] P. Sett, S. Chattopadhyay, P.K. Mallick, J. Raman Spectrosc. 31 (2000) 177–184.
[49] V. Volvosek, G. Baranovic, L. Colombo, J.R. Durig, J Raman Spectrosc. 22 (1991) 35–41.
[50] M. Muniz-Miranda, E. Castelluci, N. Neto, G. Sbrena, Spectrochim. Acta 39A (1983) 107–113.
[51] J.H.S. Green, Spectrochim. Acta 24 (1968) 1627–1637.
[52] G. Varsanyi, Assignments of Vibrational Spectra of Seven Hundred Benzene Derivatives, Wiley, New York, 1974.
[53] V.S. Madhavan, H.T. Varghese, S. Mathew, J. Vinsova, C.Y. Panicker, Spectrochim. Acta 72A (2009) 547–553.
[54] C.Y. Panicker, H.T. Varghese, K.R. Ambujakshan, S. Mathew, S. Ganguli, A.K. Nanda, C. Van Alsenoy, Y.S. Mary, J. Mol. Struct. 963 (2010) 137–144.
[55] G. Socrates, Infrared Characteristic Group Frequencies, Wiley-Interscience, New York, 1980.
[56] W. KunYi, C.W. Park, M.S. Kim, K. Kim, Bull. Korean Chem. Soc. 8 (1987) 291–296.
[57] W.B. Collier, T.D. Klots, Spectrochim. Acta 51A (1995) 1255–1272.
[58] G. Smith, D.E. Lynch, K.A. Byriel, C.H.L. Kennard, Aust. J. Chem. 48 (1995) 1133–1149.
[59] R.D. Chambers, M.A. Fox, G. Sandford, J. Trmcic, A. Goeta, J. Fluorine Chem. 128 (2007) 29–33.
[60] N. Okabe, T. Nakamura, H. Pukuda, Acta Crystallogr. C49 (1993) 1678–1680.
[61] N. Sundaraganesan, S. Ayyappan, H. Umamaheswari, B.D. Joshua, Spectrochim. Acta 66A (2007) 17–27.
[62] P. Purkayastha, N. Chattopadhyay, Phys. Chem. Chem. Phys. 2 (2003) 203–210.
[63] A. Lifshitz, C. Tamburu, A. Suslensky, F. Dubnikova, J. Phys. Chem. A 110 (2006) 4607–4613.
[64] Y.S. Mary, H.T. Varghese, C.Y. Panicker, T. Ertan, I. Yildiz, O. Temiz-Arpaci, Spectrochim. Acta 71A (2008) 566–571.
[65] A. Saeed, S. Hussain, U. Florke, Turk. J. Chem. 32 (2008) 481–486.
[66] Y.R. Shen, The Principles of Nonlinear Optics, Wiley, New York, 1984.
[67] P.V. Kolinsky, Opt. Eng. 31 (1992) 11676–11684.
[68] D.F. Eaton, Science 25 (1991) 281–287.
[69] D.A. Kleinman, Phys. Rev. 126 (1962) 1977–1979.
[70] L.N. Kuleshova, M.Y. Antipin, V.N. Khrustalev, D.V. Gusev, E.S. Bobrikova, Kristallografiya 48 (2003) 594–601.
[71] M. Adant, L. Dupuis, L. Bredas, Int. J. Quantum. Chem. 56 (2004) 497–507.
[72] E.D. Glendening, A.E. Reed, J.E. Carpenter, F. Weinhold, NBO Version 3.1, Gaussian Inc., Pittsburgh, PA.
[73] J. Choo, S. Kim, H. Joo, Y. Kwon, J. Mol. Struct. (Theochem.) 587 (2002) 1–8.
[74] R.S. Mulliken, J. Chem. Phys. 23 (1955) 1833–1840.
[75] K. Wolinski, J.F. Hinton, P. Pulay, J. Am. Chem. Soc. 112 (1990) 8251–8260.
[76] E. Scrocco, J. Tomasi, Adv. Quantum. Chem. 11 (1978) 115–193.
[77] F.J. Luque, J.M. Lopez, M. Orozco, Theor. Chem. Acc. 103 (2000) 343–345.
[78] P. Politzer, J.S. Murray, in: D.L. Beveridge, R. Lavery (Eds.), Theoretical Biochemistry and Molecular Biophysics: A Comprehensive Survey. Protein, vol. 2, Adenine Press, Schenectady, NY, 1991 (Chapter 13).
[79] E. Scrocco, J. Tomasi, Curr. Chem. 7 (1973) 95–170.